# Recent Progress in microRNA Detection Using Integrated Electric Fields and Optical Detection Methods

Logeeshan Velmanickam<sup>1</sup>, and Dharmakeerthi Nawarathna<sup>2</sup>\*

<sup>1</sup>Department of Electrical Engineering, University of Moratuwa, Moratuwa, Sri Lanka

<sup>2</sup>Department of Electrical and Computer Engineering, Old Dominion University, Norfolk, VA, 23529, USA

\*Corresponding author: dnawarat@odu.edu

### **Abstract**

Low-cost, highly-sensitivity, and minimally invasive tests for the detection and monitoring of life-threatening diseases and disorders can reduce the worldwide disease burden. Despite a number of interdisciplinary research efforts, there are still challenges remaining to be addressed, so clinically significant amounts of relevant biomarkers in body fluids can be detected with low assay cost, high sensitivity, and speed at point-of-care settings. Although the conventional proteomic technologies have shown promise, their ability to detect all levels of disease progression from early to advanced stages is limited to a limited number of diseases. One potential avenue for early diagnosis is microRNA (miRNA). Due to their upstream positions in regulatory cascades, blood-based miRNAs are sensitive biomarkers that are detectable earlier than those targeted by other methods. Therefore, miRNA is a promising diagnostic biomarker for many diseases, including those lacking optimal diagnostic tools. Electric fields have been utilized to develop various biomedical assays including cell separation, molecules detection and analysis. Recently, there has been a great interest in the utility of electric fields with optical detection methods, including fluorescence and surface plasmons toward biomarker detection. This mini review first summarizes the recent development of miRNA as a biomarker. Second, the utility of electric fields and their integration with fluorescence detection methods will be discussed. Next, recent studies that utilized electric fields and optical detection methods will be discussed. Finally, in conclusion, technology gaps and improvements needed to enable low-cost and sensitive biomarker detection in point-of-care settings will be discussed.

### A. MicroRNA as a biomarker for disease detection

Cancer, obesity and opioid abuse together pose a great threat to worldwide health. In the United States (US), it affects over 70% of the population and cost over \$250 billion per year in medical expenses [1]-[5]. A critical roadblock to combating these diseases/disorders is the lack of sensing technologies that could detect fundamental molecular changes at the cellular level related to initiation, progression of those diseases/disorders and reaction to therapeutic interventions [6]-[9]. Pancreatic cancer (PC) is one of the most lethal cancers and a major unsolved health problem worldwide [6]. About 6% of PC patients live less than five years after initial diagnosis [6]. This is in part due to the lack of a standard diagnostic tool for early detection of PC [6]. However, if this cancer was detected early and treated with existing therapy, the five-year survival rate could be 60%-100% (that is, an over ten-fold improvement). Therefore, there is an urgent need for an early detection test [6],[10],[11]. Early detection of PC involves first-use clinical risk factors (e.g., family history, age, and smoking) for identifying at-risk individuals [6]. The next step is the screening to monitor the development of PC and to determine the starting point of diagnosis and treatments [6]. There are multiple diagnostic options available for PC, including CT, MRI, and endoscopic ultrasound [6]. These modalities do not have sufficient resolution or sensitivity to be useful in the screening stage as they produce very high false-positive rates (> 90%) in screening [6],[12]. They, therefore are not recommended for frequent use in screening [6], [12]. Due to the lack of sensitivity and specificity, usage of current biomarkers (e.g., CA-19-9) is limited only to the prognosis analysis. A growing body of knowledge suggests that a potential microRNA (miRNA) biomarker panel in serum (e.g., miR-642b, miR-885-5p, and miR-22) can differentiate healthy

individuals, PC patients, and individuals in the early stage of PC development [12]. These biomarkers, in combination, represent a new avenue for the development of a clinically useful screening test.

According to the recent report from the United Nations Office of Drugs and Crime, there were about 90000 opioid related overdose deaths in North America in 2021. Every day, more than 100 people in the US die after overdosing on opioids (OUD) — a class of drugs that include the illicit drug heroin as well as licit prescription pain relievers as oxycodone, morphine and fentanyl [4]. Overdoses directly related to the misuse of and addiction to opioids, is a serious national crisis that affects public health as well as social and economic welfare [4-12]. One of the most critical issues with OUD treatment is the high relapse rate (>60%) related to non-patient-centered models that lack robust clinical tests for monitoring the efficacy of the treatments at individual level [4]-[11],[13]. Therefore, there is an urgent need for clinical tests for monitoring individual responses to treatments. The Micro-Opioid receptors (MOR) neuronal cells mediate most of the pharmacological effects of opioid drugs. Recent studies have shown that opioid drugs repress the production of MOR epigenetically through miR-23b and miR-339 [14]-[17]. The expression levels of these miRNAs in serum depend on the dose of opioid and time (after taking opioids). In contrast, the drugs (opioid antagonist) used to treat the OUD (e.g., naloxone) do not alter the miR-23b and miR-339 levels in a dose and time-dependent manner. Therefore miR-23b and 339 could be used as biomarkers for monitoring the detoxification at a personal level [14]-[17]. One potential avenue to introduce miRNA for personalizing treatments is the monitoring of miRNA levels over time (during treatments) and find the time that miRNA levels no longer alter with time. Once that time point is determined, behavioral therapy and dosage of the drug (naloxone) can be gradually decreased and the effects on relapse can be studied [14].

According to the World Health Organization (WHO), about 38% of the world population who are older than 5 years are obese [2]. Obesity is skyrocketing in the US, and over 160 million Americans are either overweight or obese [2]. Current options for defeating obesity are weight loss interventions: mainly diet and exercise or bariatric surgery. Bariatric surgery is expensive, carries significant long- and short-term side effects and often requires stringent prequalifications to be covered by health insurance [18],[19]. A combined diet and exercise program is a cheaper alternative for weight management, but there is a considerable inter-individual variability in losing weight via this method [8]. Therefore, the inability to identify the individuals who will likely succeed with diet and exercise for weight management is a critical roadblock to treating obesity [8],[18],[19]. The percentage of weight loss varies between +10.5% to -.5% for diet and exercise, and patients who cannot lose more than 5% of weight are considered non-responders [8],[20]. Dual-energy absorptiometry (DXA) is commonly used to measure body composition during weight-loss interventions but there is no clinical predictability for the success of this intervention [19]. Recent studies have shown that the expression of *miR-140* and *935* in serum at two time points about 12 weeks (preto post-intervention) apart produces a unique expression pattern in individuals who will likely lose weight and attain a healthy body weight through diet/exercise [8]. Therefore, *miR-140* and *935* can potentially be used to develop diagnostics test to profile patients who can lose weight through diet/exercise.

Cellular responses to lifestyle, stress, drugs, physiopathological conditions and pharmacological interventions have an impact on the epigenetic code, often resulting in modulation in methylome, miRNA expression, and covalent histone modifications [21]–[25]. Since epigenetic changes are taking place first in the biochemical cascade, epigenetic biomarkers could provide reliable and clinically important information, earlier than, and superior to, the downstream proteomic biomarkers [26]. It has been shown that miRNA— small non-coding RNA molecules, involve in many major cellular functions such as development, differentiation, growth, and metabolism [27]. In addition, miRNA is stably expressed in circulating blood and therefore potential candidates for health monitoring and diagnostics/screening tests [27]. As stated above, recent studies have identified unique miRNA signatures produced during the early stages of PC and treatment of OUD, as well as in response to obesity interventions [8],[12],[14]. These signatures therefore could be utilized as potential biomarkers for combating those diseases/disorders. Despite great progress in miRNA research, miRNAs have not yet been translated or used in the clinical diagnosis of any disease.

This lack of progress is partially due to the differences among and limitations of various detection technologies, which produce inconsistent results [28]. The current methods available for miRNA detection, such as Quantitative Reverse Transcription Polymerase Chain Reaction (RT-qPCR), next generation sequencing (NGS), microarray-, electrochemical-, plasmonic-, and hybridization-based miRNA sensors are not suitable for clinical screening applications. These methods do not provide absolute molarity of target miRNAs (e.g., RT-qPCR, LAMP, microarray), are inefficient for short miRNAs (e.g., NGS, RT-qPCR), have longer pre-processing times (e.g.,

microarray, electrochemical, hybridization methods), insufficient sensitivity (e.g., RT-qPCR, microarray), and low dynamic range (plasmonic, electrochemical), as well as being expensive (all) [28]–[31].

Fundamentally, nearly all-current detection methods rely on non-specific, time-dependent, and unsteady molecular diffusion for critical target-probe hybridization, causing significant variation in results [32]–[34]. Additionally, molecular crowding near detection electrodes or substrates produces steric hindrance [32]. These issues affect the sensitivity, limit of detection, and speed of detection, especially, in the detection of minute amounts (< 1%) of target miRNAs from a larger background [32]. To minimize molecular crowding, a significant dilution of serum is needed. However, a diluted serum sample (from µLs serum) is insufficient to identify miRNA signatures that are clinically important [32]-[38]. Another critical issue to overcome is the hemolysis—lysis of red blood cells during the long pre-processing time. Since some of the disease-related miRNAs are involved in the normal function of circulatory and immune systems, hemolysis could artificially increase the miRNA levels and produce inaccurate results. For example, according to reports in the literature, in tumor-associated circulating miRNAs, 58% are highly expressed in blood cells, and hemolysis alters circulating miRNA levels by about 50-fold. To minimize the hemolysis, it has been shown that a sample needs to be analyzed within 30 minutes after collection, but current pre-processing time > 4 h. Since screening or diagnosis generally depends on a single sample, this critical issue needs to be solved immediately. One way to address this issue is to introduce a rapid miRNA analysis, ideally, at point-of-care settings [39]-[41]. If these critical technical issues are solved miRNA, will be the newest pillar of medical diagnostics. Electric fields have been used in many biomedical applications including cell isolation, cell separation, and biomarker molecule (e.g., DNA, and antigens) detection. The electric fields provide ways of developing biomedical assays label-free manner. Additionally, optical detection methods, including fluorescence, surface plasmons and localized plasmons have also been utilized in the detection of biomarker molecules. Fluorescence has been the method of choice for many biomarker detection methods.

## **B.** Fluorescence Spectroscopy for Biomarker Detection

Fluorescence is an optical phenomenon in which some molecules (fluorophores or fluorochromes) absorbed light energy and excited to a higher energy state, called excited energy. Since these molecules cannot sustain the excited energy state for very long, they decay to a lower energy state by emitting light energy; this process is called fluorescence. Fluorescence spectroscopy or fluorometry or spectro-fluorometry is a category of electromagnetic spectroscopy that examines the fluorescence emission of a sample [42]–[47]. Fluorescence spectroscopy is a popular research tool that is commonly used in biochemistry, molecular biology, and biomedical applications for medical diagnosis. Moreover, fluorescence spectroscopy has been used in applications such as DNA sequencing, single biomolecule sensing, mineralogy, and genomics [42]–[44],[46]. Almost all characteristic features of the fluorescence, including spectral offsets, quantum yields, lifetimes, fluorescence quenching and anisotropies, have been utilized in fundamental and applied research and detection assays [46],[47].

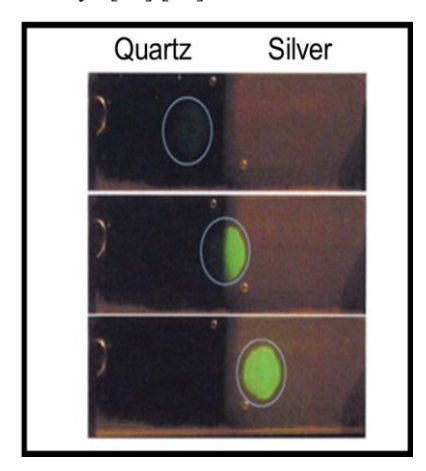


Fig. 1: Fluorescence enhancement from silver nanostructures. Photographs of fluorescein-labeled human serum albumin (molar ratio of fluorescein/ human serum albumin = 7) on quartz and on Silver fractal-like structures. Fluoroscence was observed with 430 nm excitation and 480 nm long-pass filter. The excitation was progressively moved from the quartz side to the silver side. This figure was extracted from ref [48] and [49] with permission.

The inclusion of fluorescence as a part of biosensing has led to tremendous growth in both biosensing and fundamental fluorescence studies. As a result, optical bio-sensors have paved the path toward the advancement of highly sensitive, strong, and facile detection of target biomarkers [50],[51]. To use fluorescence in the detection, labeling of target molecules with fluorophore tags is needed, and then fluorescence intensity is measured. Later, the fluorescence intensity is converted to molarity values [50],[52]–[54]. In sensing applications of biomolecules, there are three fundamental parameters used to determine the applicability of the sensing method to a specific application. These are sensitivity, specificity, and limit of detection [55]. Although sensitivity and specificity of fluorescence-based detection are very high, the limit of detection could be further improved to be applicable in many medical applications. For example, studies have reported that the current detection limit of fluorescence-based detection is not sufficient to detect many disease-related biomarkers, particularly for detecting early-stage disease development [56]–[58].

To further improve the detection limit of the fluorescence-based assays, near-field metal-fluorophore interactions could be used (Fig. 1). For example many studies including Fu et al. [59], White et al., [60], Choudhury et al. [61], and others have used near-field metal-fluorophore interactions to enhance the fluorescence intensity. Moreover, studies have reported that metal (e.g., silver and gold) could alter the characteristic features of properties of fluorophore molecules; these changes have led to increased fluorescence intensity and stability of fluorophore molecules. We will briefly discuss some of these properties below.

The quantum yield of a fluorophore is an important parameter in fluorescence measurements, which gives the efficiency of the fluorescence process [62]–[64]. This can then be simply expressed as the ratio between the numbers of photons emitted to the numbers of photons absorbed. The highest quantum yield of a fluorophore is 1 (100%) when the photon absorbed is equal to the photon emitted [62]–[64].

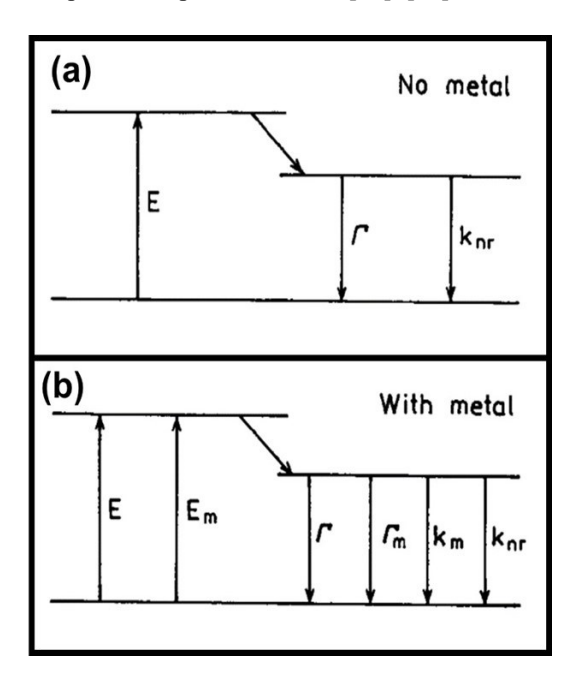


Fig. 2: Jablonski diagram without (a) and with (b) the effects of a nearby metal surface. For metal-fluorophore distances over 5 nm, the effect of quenching by the metal  $(k_m)$  is expected to be minimal. This figure was adapted from ref [62] with permission.

We can demonstrate the quantum yield through the Jablonski diagram (Fig. 2). Moreover, the quantum yield and lifetime of a fluorophore are dominated by the magnitudes of the radiative rate ( $\Gamma$ ) and the sum of the non-radiative decay rate ( $k_{nr}$ ) [62],[63]. The quantum yield ( $\emptyset_0$ ) of the fluorophore in the absence of quenching can be represented as:

$$\emptyset_0 = \frac{\Gamma}{\Gamma + k_{nr}} \tag{1}$$

The lifetime of a fluorophore  $(\tau_n)$  without metal is the inverse of the radiative decay rate  $(\tau_n = [\Gamma + \text{knr}]^{-1})$  [62],[63]. When metal is present near a fluorophore molecule, the quantum yield can be written as:

$$\phi_m = \frac{\Gamma + \Gamma_m}{\Gamma + \Gamma_m + k_{nr}},\tag{2}$$

where  $\Gamma_m$  represents the radiative decay rate increase due to the presence of metal nanostructures (hotspots) or metal thin films. Then, the lifetime of the fluorophore is  $(\tau_n) = (\Gamma + \Gamma_m + k_{nr})^{-1})$  [62]–[64]. Therefore, presence of metal could increase the quantum yield and decrease the lifetime of the fluorophore; both of these effects will make the fluorophores very bright and stable. At fundamental level, increasing the radiative decay rate of fluorophore molecules is highly dependent on the ability to orient the fluorophore dipole with the plasmonic axis of the hotspots and subsequently place the fluorophore molecules in the area with the highest density of surface plasmon. For example, this effect is maximum when the fluorophore molecule is perpendicular to the surface of an ellipsoidal nanostructures that has  $\left(\frac{a}{b}\right)$  ratio equal to 1.75; the radiative decay rate of the fluorophore could be increased by a factor of 1000-fold or greater [62],[64].

The presence of metal could alter the apparent quantum yield (Y) of the fluorophore molecules, which is defined as the intensity of the fluorophore relative to the control sample (without metal surface) measured with the same intensity of excited light. Mathematically, Y can be represented as

$$Y = \left| L_{(\omega_{ex})} \right|^2 Z_{(\omega_{em})},\tag{3}$$

where  $L_{(\omega_{ex})}$  is the product of the fluorophore quantum yield without metal, and the amplification of the incident field  $\left(\frac{E}{E_0}\right)$  by the metal;  $Z_{(\omega_{em})}$  represent the partition of energy into the radiative and non-radiative decay pathways, as modified by the metal particles (Fig. 3) [62]. The electric field enhancement could be due to the light scattering near nanostructures or hotspots. In addition, since the fluorescence intensity depends on the square of the electric field enhancement  $\left(\frac{E}{E_0}\right)$ , metal structures can significantly enhance the intensity of the fluorophore relative to the control sample. Studies have reported that the electric field enhancement due to the metal surfaces can be as high as 140 [62]. To achieve large enhancement of fluorescence intensity, the fluorophore should be placed 5–20 nm from the metal surfaces or nano-structures [62]–[64].

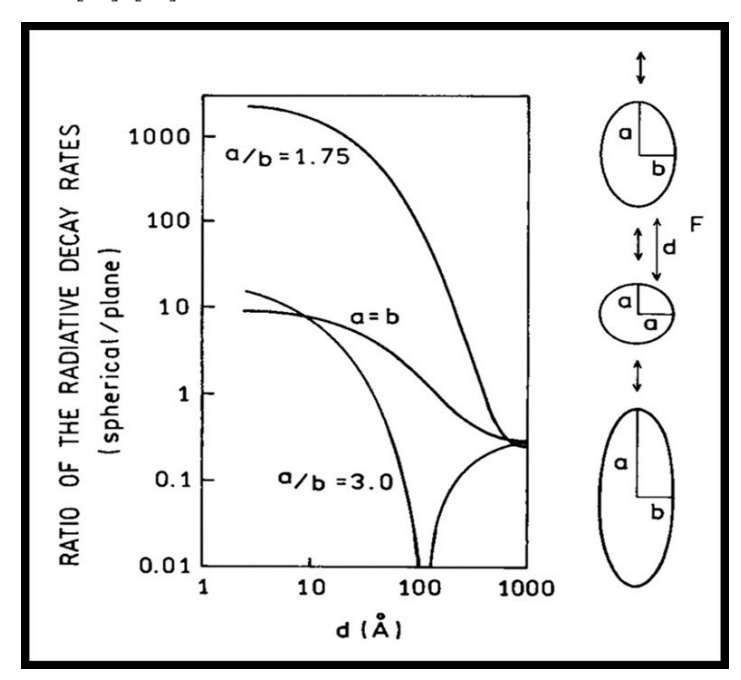


Fig. 3: The effects metallic nanostructures on the radiative decay rate of a fluorophore. The volume of each spheroid is equal to a sphere with 40 nm diameter. This figure was adapted from ref [62] with permission.

As stated above, the presence of metal can have detrimental effects, such as fluorescence quenching on fluorophores. Quenching refers to any process that results in a decrease in the fluorescence emission intensity [62],[65]–[67]. During the quenching process, the fluorophore returns to the ground state, without emitting energy or a photon. The quantum yield  $(\emptyset_0)$  of a fluorophore with quenching can be represented as:

$$\emptyset_0 = \frac{\Gamma}{\Gamma + k_{nr} + k_q[Q_u]} \tag{4}$$

 $k_q[Q_u]$  represents the quenching rate [62],[68]. The quantum yield of a fluorophore in the presence of a metal surface  $(\emptyset_m)$  can be represented as

$$\phi_m = \frac{\Gamma + \Gamma_m}{\Gamma + \Gamma_m + k_{nr} + k_m},\tag{5}$$

where the  $k_m$  refers to the quenching effect by the metal surface. Because of the quenching effect, the lifetime of a fluorophore can be defined as  $(\tau_n) = [\Gamma + \Gamma_m + k_{nr} + k_m]^{-1}$  [62],[63]. The quenching effect could decrease both quantum yield and the lifetime of a fluorophore. As a result, quenching will significantly decrease the fluorescence intensity. One way to minimize the quenching is to increase the metal-fluorophore distance [62]-[64],[69].

As we discussed above, the fundamental mechanisms responsible for the fluorescence enhancement are:

- (a) Decreasing fluorophore quenching by reducing the energy transfer from fluorophore molecules to the metal or increase the metal-fluorophore distance,
- **(b)** Increasing the radiative decay rate of fluorophore molecules by aligning the fluorophore dipole with the plasmonic axis and placing the fluorophores in the high surface plasmonic region, and
- (c) Concentrating the fluorophore molecules in an area where a local electric field is produced from light scattered by plasmonic structures [49],[62],[70].

Under optimized conditions, mechanism (a) eliminates the fluorophore quenching, mechanism (b) contributes about  $10^5$  times (maximum), and mechanism (c) contributes about  $10^4$  times (maximum) to the fluorescence enhancement [49],[62],[70]. Therefore, if mechanisms (a), (b) and (c) are integrated, a maximum of one-billion-fold fluorescence enhancement is possible to achieve. Billion-fold enhancement will easily produce the detection of few fluorophore molecules. Unfortunately, there were no studies that focused on developing strategies to integrate these mechanisms with solutions that are easily implemented in point-of-care settings [62]. In the upcoming sections, we will discuss the avenues of using electric fields (<10 MHz) to enhance the fluorescence intensity. One of the potential avenues associated with electric field is the dielectrophoresis of molecules which can potentially be used to optimize the effects of the fluorescence enhancement mechanisms indicated above and achieve significantly large fluorescence enhancement.

In addition to fluorescence spectroscopy, Surface-Enhanced Raman Spectroscopy, Surface Plasmon Resonance and Localized Surface Plasmon Resonance techniques offer promising avenues for biomarker detection. Surface-enhanced Raman scattering (SERS) is a phenomenon that significantly enhances the Raman signal of molecules when they are in close proximity to nanostructured metallic substrates [159-161]. This enhancement arises from two main mechanisms: electromagnetic and chemical effects. The electromagnetic enhancement ( $G_{\rm EmSERS}$ ) results from the localization of light at the surface of the substrate, leading to strong spatial amplification of the incident laser light in small regions called hot spots [159]. This amplification increases the local electric field experienced by the molecules, enhancing their Raman scattering signal. Additionally, the presence of the metallic structure modifies the efficiency with which the molecules radiate Raman power, further contributing to the enhancement. The chemical enhancement ( $G_{ChemSERS}$ ), on the other hand, stems from the modification of the polarizability of the molecules due to their interaction with the substrate [159-160]. While the electromagnetic enhancement is independent of the type of molecule and can reach extremely high values, the chemical enhancement depends on the specific molecule-substrate interaction and is typically smaller in magnitude.

The electromagnetic enhancement arises from two main mechanisms: local field enhancement and re-radiation enhancement. The local field enhancement is quantified by the square of the ratio of the local electric field to the incident electric field at both the excitation laser frequency and the Raman frequency[159].

For SERS to effectively utilize these enhancements, it's essential to grasp the maximal potentials. Studies have outlined approximate maximal values fo  $G_{EmSERS}$  and  $G_{ChemSERS}$ , offering insights into the immense amplification

capacity of SERS. Averaged over the substrate,  $G_{EmSERS}$  reaches  $10^8$ , while in localized "hot spots," it surges to  $10^{10}$ . Comparatively,  $G_{ChemSERS}$  achieves approximately  $10^2$  for effects tied to atomic-scale roughness and peaks at  $10^4$  for phenomena related to charge transfer resonance [159].

These maximal values underscore the transformative potential of SERS in highly sensitive molecular detection and analysis, providing invaluable insights into molecular interactions and surface phenomena.

Surface Plasmon Resonance (SPR) and Localized Surface Plasmon Resonance (LSPR) techniques operate based on the principles of exciting and detecting surface plasmons, which are collective oscillations of free electrons at the interface between a metal and a dielectric medium, typically a prism or a glass substrate coated with a thin metal film (usually gold or silver) [162-164].

In SPR, a collimated beam of monochromatic light, typically from a laser, is directed onto the metal-dielectric interface at a specific angle known as the resonance angle [162]. When the incident light matches the resonance angle, it couples with the surface plasmons, leading to a reduction in reflectivity of the light. This reduction is detected as a dip in the reflectance curve, which is highly sensitive to changes in the refractive index of the medium adjacent to the metal surface [162,163]. When biomolecules bind to receptors immobilized on the metal surface, they induce changes in the refractive index, causing a shift in the resonance angle or a change in the shape of the reflectance curve. By monitoring these changes, SPR can provide real-time information about biomolecular interactions, including binding kinetics, affinity constants, and analyte concentrations[162].LSPR, on the other hand, relies on the interaction of light with metallic nanoparticles, such as gold or silver nanoparticles [164]. When nanoparticles are illuminated with light of a specific wavelength, the collective oscillations of free electrons in the nanoparticles result in a resonance phenomenon known as LSPR[164]. This localized resonance leads to enhanced electromagnetic fields in the vicinity of the nanoparticles, which can be exploited for sensing applications.

C. In both SPR and LSPR, the sensitivity of the technique depends on factors such as the refractive index of the medium near the metal surface, the size, shape, and material properties of the nanoparticles (in the case of LSPR), and the quality of the immobilized receptors on the sensor surface [163]. By optimizing these parameters and employing signal amplification strategies, such as nanoparticle functionalization or secondary detection with labeled molecules, the sensitivity and specificity of SPR and LSPR techniques can be further enhanced [162-164]. Dielectrophoresis: Utility of Electric Fields to Detect Circulating Biomarkers

The term dielectrophoresis (DEP) was first used by Phol in 1951, derived from the Greek word "phorein", an effect where a particle is carried as a result of its dielectric properties [72]. First, Phol defined this effect as "the motion of suspensoid particles relative to that of the solvent resulting from polarization forces produced by an inhomogeneous electric field" [72] [73]. Any material, which can be polarizable when its subject to an exterior electric field is known as dielectric [74]. When a dielectric material is placed in an applied exterior electric field, electric charges do not pass through them due to the electrical insulator characteristic; only the electric charges deviate slightly from their average equilibrium positions, which cause a dielectric polarization in the dielectric materials [73],[75],[76]. Due to the polarization of the dielectric material, electric dipoles are produced in the dielectric materials [77],[78]. DEP is produced on a suspended dielectric particle in a buffer solution when an exterior non-uniform electric field polarizes the particle; the polarized dielectric particles experience a force called dielectric particle located in a non-uniform electric field region can be represented by the equation (6).

$$F_{DEP} = \frac{1}{2} \alpha \, \nabla |E|^2 \tag{6}$$

where  $\alpha$  is the polarizability of the dielectric particle,  $\nabla$  is the vector operator, and E is the RMS value of the electric field. The  $\alpha$  or polarizability of the suspended dielectric particle depends on the frequency and field dependent dielectric properties of particle and the suspended medium [73],[76],[79]–[89]. The DEP force can be attractive or repellent from electrodes based on the value of  $\alpha$ . The attractive DEP (positive DEP) produced when  $\alpha$  is positive and the DEP force move the dielectric particle towards electrode edges or to the higher electric field gradient region or to the region that has maximum value for  $\nabla |E|^2$ ; similarly, repulsive DEP (negative DEP) is produced when  $\alpha$  is negative and DEP force move the particle in the opposite direction of the higher electric field gradient and to the weak electric field gradient (Fig. 4) [72], [75], [79], [90].

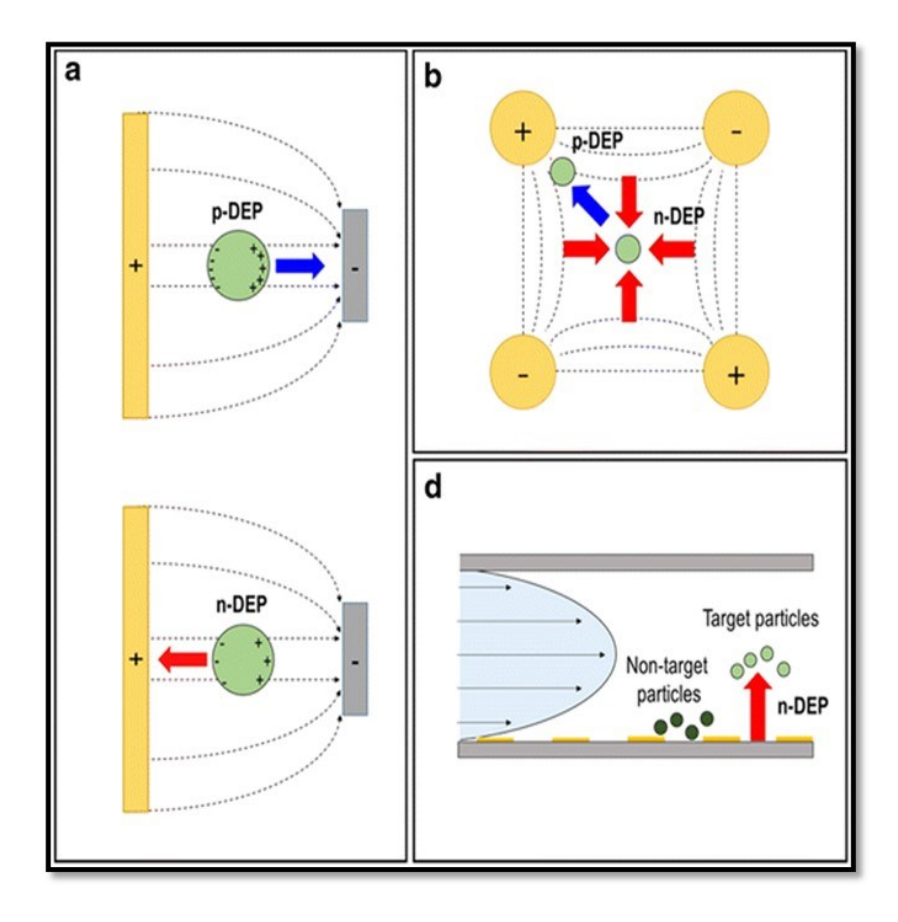


Fig. 4: (a) Traditional DEP force can be used to concentrate particles near electrodes using positive or negative DEP force, (b) another electrode configuration to concentrate particles either on electrodes, or away from electrodes, (c) integration of DEP force with viscous drag force for continuous separation of particles. This figure was adapted from ref [90] with permission.

The polarizability of a spherical particle can be derived as:

$$\alpha = 4\pi r^3 \varepsilon_m Re[f_{CM}(\omega)] \tag{7}$$

where is the radius of the spherical dielectric particle,  $\varepsilon_m$  is the permittivity of the suspending medium,  $\omega$  is the radial frequency of the applied electric field, and  $\mathbf{Re}\{f_{CM}(\omega)\}$  is the real part of the Clausius-Mossotti factor (CM) and for the spherical particle, is defined as:

$$f_{CM}(\omega) = \frac{\varepsilon_p^* - \varepsilon_m^*}{\varepsilon_p^* + 2\varepsilon_m^*} \tag{8}$$

where  $\varepsilon_p^*$  is the complex permittivity of the dielectric particle and  $\varepsilon_m^*$  is the complex permittivity of the suspending medium. The complex permittivity is given by  $\varepsilon^* = \varepsilon - j(\frac{\sigma}{\omega})$  with  $\sigma$  the real conductivity,  $\varepsilon$  the real permittivity, and  $j = \sqrt{-1}$  and  $\omega$  the angular frequency [72],[73],[79],[84]-[89],[91]-[99].

Variations in the CM factor alter the value of  $\alpha$  and subsequently vary the DEP force. For example, for a sphere, the real part of the CM factor is theoretically bounded between -1/2 and 1. Moreover, we can re-define positive DEP and negative DEP. Positive DEP occurs when  $Re[f_{CM}(\omega)] > 0$  and negative DEP occurs when  $Re[f_{CM}(\omega)] < 0$ . If  $Re[f_{CM}(\omega)]$  becomes zero under certain conditions, the DEP force act on the polarized particles also becomes zero [91]–[96],[99]. The frequency at which zero DEP force occurs is called crossover frequency ( $f_{CO}$ ), which is defined as:

$$f_{CO} = \frac{1}{2\pi\varepsilon_0} \sqrt{\frac{(\sigma_m - \sigma_p)(\sigma_p + 2\sigma_m)}{(\varepsilon_p - \varepsilon_m)(\varepsilon_p + 2\varepsilon_m)}},$$
 (9)

where  $\sigma$  is the real conductivity and  $\varepsilon$  is the real permittivity, and sub-index p, m are the particle and medium respectively [73],[91],[99],[100]. The conductivity ( $\sigma_p$ ) of the homogeneous dielectric spherical particle can be written as the sum of bulk conductivity ( $\sigma_{pbulk}$ ) and surface conductance ( $K_S$ ), which can be represented as:

$$\sigma_p = \sigma_{pbulk} + \frac{2K_S}{r},\tag{10}$$

where r is the radius of the spherical particle. Depending on the material of the particle, such as polystyrene and silica, the bulk conductivity ( $\sigma_{pbulk}$ ) can be negligible. Therefore, surface conductance ( $K_S$ ) provide a dominating contribution to the conductivity of the particle [73],[91],[96],[99],[100].

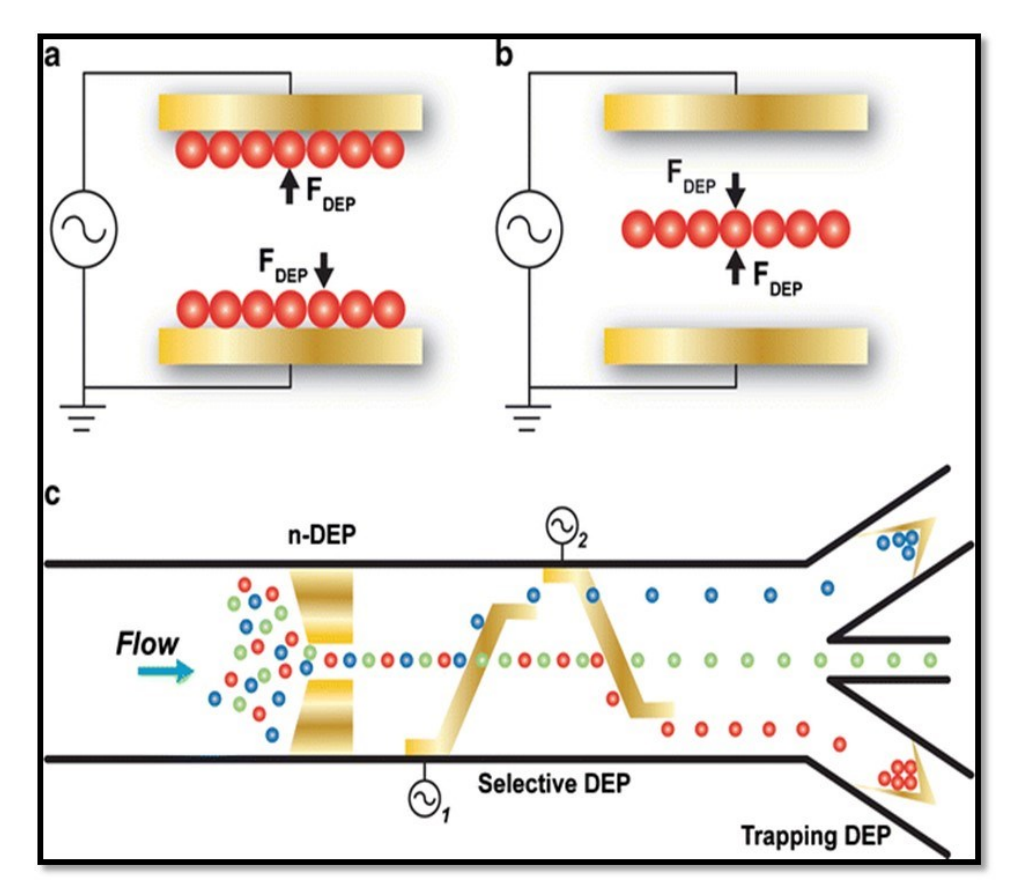


Fig. 5: (a) Trapping particles with positive DEP force. (b) Trapping particles using negative DEP force and (c) Use DEP force (positive and/or negative) of particles in microfluidic systems for separating particles. This figure was adapted from ref [101] with permission.

DEP force has been used in sensing, trapping, transporting, and sorting different type of dielectric particles (Fig. 5) [73],[102]. In Fig 5(c), the electrode design plays an crucial role in creating a non-uniform electric field within microfluidic systems. This electric field is engineered to selectively manipulate particles based on their dielectric properties. By employing electrodes strategically positioned along the microfluidic channel, the design facilitates the trapping and separation of particles. Target particles, responsive to positive DEP, are drawn towards the electrodes and effectively trapped, while non-target particles, experiencing negative DEP or minimal DEP, continue their flow through the channel. Since the biological samples, such as cells, proteins, DNAs, RNAs, and miRNAs are considered as dielectric particles, they can use in DEP studies. The earliest dielectrophoretic studies were largely conducted with the aim of understanding how cells produce DEP forces, and how to use DEP and dielectric

properties of cells to better understanding their physicochemical properties [73],[102]–[104]. Currently, DEP has made it possible to achieve: separation of cancer cells from healthy cells [73],[102],[105], [154]; separation dead cells from live cells [106],[107]; high speed cell sorting [102],[103]; cell patterning [102],[104],[108],[109], [155]; rotation of cells [156-158], and electroporation [73],[81],[102].

Positive and negative dielectrophoretic phenomenon utilized in the separation of cells or particles. A selected frequency of the signal will be applied to the particle sorting device, where the target particles will feel the positive DEP and become trapped at the electrodes; at the same time nontarget particles experience negative DEP (or repulsive DEP from electrodes) or zero DEP force, and flow out without trapping (Fig. 5). Finally, the trapped target particles were released from the electrodes by switching off the field and collected separately. In addition, there are other methods that combine DEP trapping with viscous drag force used to separate materials continuous fashion [99],[102],[103],[110]. In addition to cells, biomarker molecules (such as DNAs, proteins, and RNAs) were trapped on the electrodes using DEP force for calculation of expression levels or molarities [85],[111] [112]. In addition, high-speed hybridization of DNAs and RNAs was also successfully conducted using the DEP force, and this might drastically improve the biological assay time [113],[114]; these developments collectively advanced the biosensing techniques involved in the detection of rare biomarkers in biological, environmental, and other samples [73],[112]. Studies have also focused on using DEP in biomarker sensing applications [115]. With the introduction of DEP in biosensing, critical sensing parameters such as sensitivity, specificity, and detection limit have significantly improved [58],[112]. For example, the miRNA molecules, which are short in size (~8 nm) and represent a biomarker for early-stage cancers, have been successfully detected using DEP and proved to be superior to the other current detection techniques available in the medical industry [112].

In addition to the medical applications, DEP has also been widely used in other industrial applications, such as separating minerals [116]–[118], self-recovering current limiting fuse [119], depositing a patterned coating of a nanostructure material onto a substrate [73],[120], collecting of micron-scale particles (granular, threadlike, sheets, or microelectronic parts) [73][121], polishing local areas of 3D surfaces using abrasive powders [73],[122], biodegradation of organic pollutants in soil [73],[123], and in water treatments systems [73],[124]. During the separating of minerals, DEP is applied at different frequencies and based on the frequency, the polarizability of the mineral particles' changes. Because of these polarizability changes, the minerals are separated from each other using the DEP force [116],[117],[125]. In self-recovering current limiting fuse, the current-limiting operation was attained by frequently switching between a conducting position, collection of conductive particles between two electrodes brought by DEP, and evaporation or spreading state of the conductive particles due to Brownian motion or diffusion [73].

In the process of coating a nanostructure material onto a substrate, an AC potential applied between two electrodes for a time limit period. The applied AC potential create a DEP force on the nanostructure materials suspended in the solution and them to the electrodes [73],[119]. The polishing of 3D surfaces was achieved by abrasive powders, such as Al<sub>2</sub>O<sub>3</sub>, diamond or SiC, dispersed in silicone oil and agitated by DEP forces similar to the coating process [72],[121]. In the water treatment systems, the live bacteria and microbes in water were selectively concentrated and separated by the nature of the polarizability of the particle due to the DEP force in different frequencies [72],[123].Advances in the use of DEP for manipulation of nanoparticles are also opening up new applications, including the fabrication of a new generation of electronic devices and sensors [73]. In addition to the traditional metal electrode-based DEP studies, the electrode-less DEP has also been developed and used in multiple studies [85],[125]–[127]. The electrode-less DEP could be produced on the molecules that are suspended in the physiological buffers, such as blood, serum, and urine [85],[127]; it could further simplify the assays.

When fluorescence enhancement can potentially integrate with electric fields and DEP, the fluorescence enhancement could be increased well beyond the current limits. Traditional fluorescence enhancement studies use the diffusion of molecules or a combination of diffusion and sample flow to concentrate fluorophore molecules in hotspots [128]. Diffusion is not a selective or steady state process for selectively concentrating target biomarker molecules. Since the diffusion is not a steady state process, it produces results with a large degree of inter-sample variability. The introduction of DEP could provide a selective method for concentrating biomarker molecules in hotspots for detection. In addition, below, we will discuss a potential avenue for electric fields and DEP force to be used to integrate fluorescence enhancement mechanisms (a), (b) and (c) (indicated above) as well as to eliminate or minimize fluorophore quenching.

### D. Utility of Electric Fields to Enhance the Near-field Fluorescence Enhancement Mechanisms

Studies have shown that energy transfer from fluorophores to metal quench the fluorescence (**mechanism** (a) discussed under the title Fluorescence spectroscopy for biomarker detection), which is effective for the fluorophores that are located within about 5 nm from the metal edges of hotspots [70],[129]. When dielectrophoresis is used to concentrate molecules in hotspots, fluorophore-labeled biomarker molecules (e.g., miRNA) are fully stretched by the high-electric fields in the hotspots. Therefore, for example, miRNA molecules will form rod-like shapes that are about 8 nm long (each base pair is about 4 Å long) and 2 nm in diameter. When the biomarker molecule experiences dielectrophoresis, it rotates such that the dipole along the longest non-dispersed axis aligns with the field [129], [130]. Therefore, the long axis of the rod will be aligned with the field [129].

The dipole moment of biomarker molecules is larger than the fluorophore molecules at low frequency. For example, dipole moment of miRNA molecules are about 10 times larger than typical fluorophores (e.g., fluorescein and cyanine 3 (Cy3)) [129],[131]. Therefore, miRNA molecules have about 10-times larger polarizability ( $\alpha$ ) than fluorophores [132]. Since the polarizability is directly proportional to the dielectrophoretic force, miRNA molecules experience larger DEP force than fluorophore molecules. Therefore, the miRNA portion is attracted to the region with the largest electric field gradient ( $\nabla(E^2)$ ). Since the largest electric field gradient is produced near the electrodes, miRNA molecules will be located closer to the metal edges of the hotspots [132]. As a result, fluorophore molecules will be located about 8 nm from the metal edges. As a result, the introduction of dielectrophoresis aligns the fluorophore molecules outside the active region of fluorophore quenching. This ability is highly significant for detecting low miRNA concentrations. Similar arguments can be made for the antigen and other nucleic acid biomarker molecules.

The fluorescence enhancement expected from increasing the radiative decay rate (mechanism (b)) is highly dependent on the ability to orient the fluorophore dipole with the plasmonic axis of the hotspots and subsequently place the molecules in the area that has large amount of surface plasmons [64],[70]. When dielectrophoresis is used to concentrate the fluorophore-labeled biomarker molecules (e.g., fluorophore labeled miRNA molecules), the electric field gradient and electric polarization produced by the external electric potential on the molecules is used [132]. Metal nanostructures can be approximated as a dipole [133]. Therefore, the highest electric field and the field gradient will be produced along the dipole axis [134]. Typically, this dipole is formed in the sharp edges of the nanostructures [132]. As a result, fluorophore-labeled biomarker molecules will be aligned along the electric dipole axis. When fluorophore molecules are excited with the appropriate wavelength of light, even though the frequency values are different, if the surface plasmon dipoles is also produced in the same locations as the electric dipole, fluorophore molecules can be aligned with plasmon dipole axis. Therefore, when dielectrophoresis is used to concentrate fluorophore molecules, fluorophore dipole of each molecule could be aligned with the plasmonic dipole axis of the hotspots. This is critically important in enhancing fluorescence because studies have shown that wellaligned fluorophores with the plasmonic axis could enhance the fluorescence by up to a few thousand times. In addition, dielectrophoresis can be used to vary the fluorophore-metal distance to concentrate the fluorophores in the high surface plasmonic region. Briefly, first, attractive dielectrophoresis concentrate molecules near the metal edges of the electrodes and apply repulsive dielectrophoresis to push the concentrated molecules away from the electrodeedges to the lowest field gradient region [82],[135]. One can record fluorescence intensity of the sample as the molecules are being pushed from metals edges. Finally, the distance that produces the largest fluorescence intensity can be found. The two effects that are related to mechanism (b) combine to produce about 105 times enhancement of fluorescence.

The contribution from **mechanism** (c) depends on the ability to concentrate the fluorophores in an area where there is a large electric field produced by scattered light near the hotspots [62],[128]. Since sizes of the nanostructures are below 100 nm, significantly large electric field distribution is expected in the hotspots. Moreover, fluorescence enhancement is proportional to the square of the electric field enhancement. To enhance the fluorescence, fluorophore labeled biomarker molecules must be placed in the region that has the largest electric field enhancement [62]. The dielectrophoresis of fluorophore labeled biomarker molecules can be used to concentrate the molecules in the high electric field regions. As stated above, the distance between the fluorophore-metal edges will be altered using a combination of attractive and repulsive dielectrophoresis. This effect will have a maximum of 10 <sup>4</sup> fold enhancement of fluorescence. For these reasons, the introduction of dielectrophoresis could potentially approach the theoretical limit of about one billion-fold (10<sup>4+5</sup>) enhancement. In theory, billion-fold enhancement translates to increasing fluorescence intensity of one fluorophore molecules to the fluorescence intensity of billion fluorophore molecules. Therefore, the detection of just a few fluorescently labeled molecules without complicated machinery, cost, or capital will be possible. This would be ideal for the detection of early-stage diseases in point-of-care settings. Next, we will discuss recent studies and devices that utilized integrated electric fields and optical detection

methods, including fluorescence enhancement to detect biomarker molecules in clinical samples. We have surveyed the recent published studies that utilized electric fields and optical detection methods, including enhanced fluorescence and discussed the few studies to highlight the utility of electric fields with optical detection methods.

## E. Integrated Electric Fields and Optical Detection Methods for Biomarker Molecular Detection

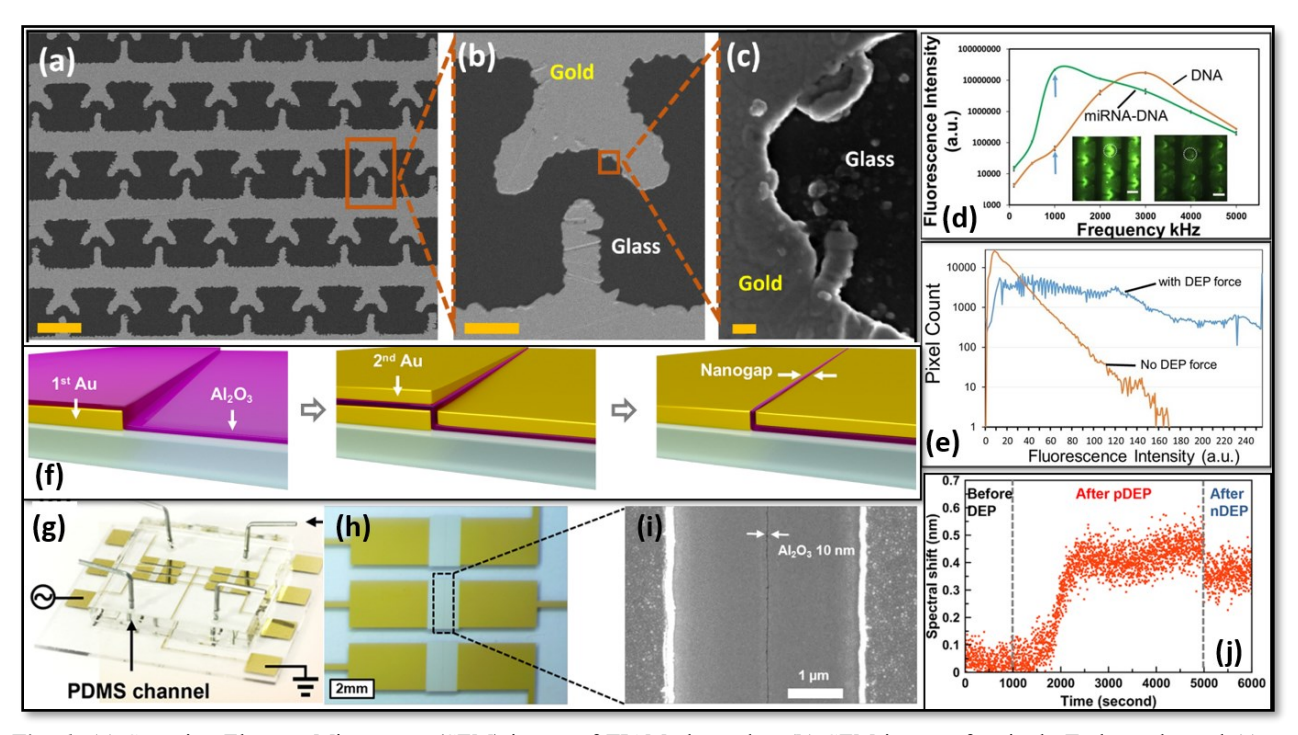


Fig. 6: (a) Scanning Electron Microscope (SEM) image of TIAM electrodes, (b) SEM image of a single T-electrode, and (c) SEM images of hotspots. (d) Fluorescence intensity variation with the frequency of applied external potential for miRNA-DNA and DNA molecules. Blue arrows indicate fluorescence intensities at 1 MHz, with insects showing fluorescence images with miRNA-DNA (bright) and without miRNA (dark) molecules (scale bars: 50 μm). (e) Fluorescence intensity of the sample with and without DEP force. (f) Device fabrication via atomic layer lithography, including batch fabrication of trench resonators. (g) A picture of six-device chip with Polydimethylsiloxane (PDMS) microfluidics. (h) optical-microscope image of the chip, and (i) top-down SEM of trench resonator. (j) Spectral shift as bovine serum albumin molecules (10 pM concentration) are trapped with positive DEP bias of 5 V and 1 kHz frequency, followed by a 0 MHz frequency application after 5000 s, leading to negative DEP. With permissions from publishers, images labeled (a-c) were extracted from [153], (d) was extracted from [111], (e) was extracted from [138], and (f-j) were obtained from [140].

Velmanickam Logeeshan et al. reported on a miRNA detection device (iLluminate-miRNA platform) for point-of-care applications. iLluminate-miRNA platform utilizes microscale and nanoscale metallic structures to achieve rapid and sensitive miRNA detection [111]. The fabrication of the device involved the creation of a T-shaped interdigitated array of microelectrodes (TIAMs) with nanoscale plasmonic hotspots (Fig 6: (a-c)). The nanoscale hotspots produced large electric field gradients of approximately  $10^{17}$  V<sup>2</sup>/m<sup>3</sup> [111]. Large electric field gradient produced strong DEP force on the fluorophore labeled target miRNAs or fluorophore labeled miRNA-DNA duplexes and concentrated them on the electrodes. The study used the fluorescence enhancement mechanisms discussed and detected very low levels of miRNA levels. Experimental results demonstrated the detection of miRNA in serum samples (Fig 6:(d)). Importantly, iLluminate-miRNA platform demonstrated superior sensitivity when compared to conventional methods. The detection limit of the iLluminate-miRNA was few fM [111]. This technique holds a promise for future clinical applications and warrants further investigation to optimize specificity and explore its potential in measuring miRNA cancer biomarkers.

Velmanickam Logeeshan et al. presented an extension of their previous study, introducing a method to amplify the fluorescence intensity of fluorophore molecules using AC electric fields [138]. This study emphasizes the technique's potential in developing highly sensitive biosensors for clinical applications. This study addressed the challenge of detecting weak fluorescence intensities from a few target biomarker molecules by enhancing the fluorescence intensity using low-frequency electric fields. The electric fields were utilized to minimize fluorophore quenching, increasing the radiative decay rate (RDR), and concentrating molecules with DEP force in the local plasmonic hotspots and harnessing energy from the excitation source (Fig 6: (e)). Additionally, the authors draw from Nitzan and Gerten's initial studies to develop an electromagnetic model predicting enhancement based on hotspot properties and distance [139]. Their calculations indicate an approximate 50-fold enhancement. As RDR increases, fluorophores become more stable, allowing for an additional 50-fold increase in illumination intensity, resulting in a total enhancement of 2,500-fold [138]. Therefore, by combining all the mechanisms provided, the research results in about 6 × 10<sup>8</sup> fold fluorescence enhancement [138].

Dehan Yoo et al. reported on a study on the integration of plasmonics and electronics using a split-trench resonator platform [140]. This platform combines high-quality-factor resonant plasmonic biosensors with radio frequency (RF) nanogap tweezers, enabling dielectrophoretic trapping of analytes. These researchers utilized a scalable fabrication process, involving photolithography and atomic layer deposition, to create centimeter-long trench resonators with sub-10 nm gaps. To fabricate the device, photolithography was used to transfer rectangular patterns onto a photoresist-coated wafer followed by metal deposition and lift-off to form the first Au rectangular hole patterns [140]. Subsequently, a conformal coating of Al<sub>2</sub>O<sub>3</sub> was applied using atomic layer deposition. Directional evaporation was utilized to deposit a second Au film, filling the rectangular hole patterns. The excess second Au film was then removed, resulting in vertically oriented Al<sub>2</sub>O<sub>3</sub> gaps along the perimeter of the patterns. This process was followed by additional lithography steps to create nanogap patterns and a trench structure (Fig 6: (f-i)). Finally, a 1 µm thick Ag layer was deposited using electron-beam evaporation to create a trench along the gap. The key highlight of this study was the successful integration of DEP with nano-plasmonic sensing. By applying an RF electrical bias across the 10 nm gap, strong electric field gradients were generated for efficient trapping of nanoparticles and proteins [140]. The trapped analytes were then detected using refractive-index sensing by leveraging the interference between surface-plasmon standing waves and transmitted light through the nanogap. The platform demonstrated remarkable sensitivity and detected the analytes as low as 10 pM (Fig 6: (j)) [140]. The integration of DEP in the split-trench resonator platform offers numerous advantages, including enhanced analyte transport and rapid detection capabilities. Compared to traditional diffusion-limited methods, this platform significantly reduces detection times.

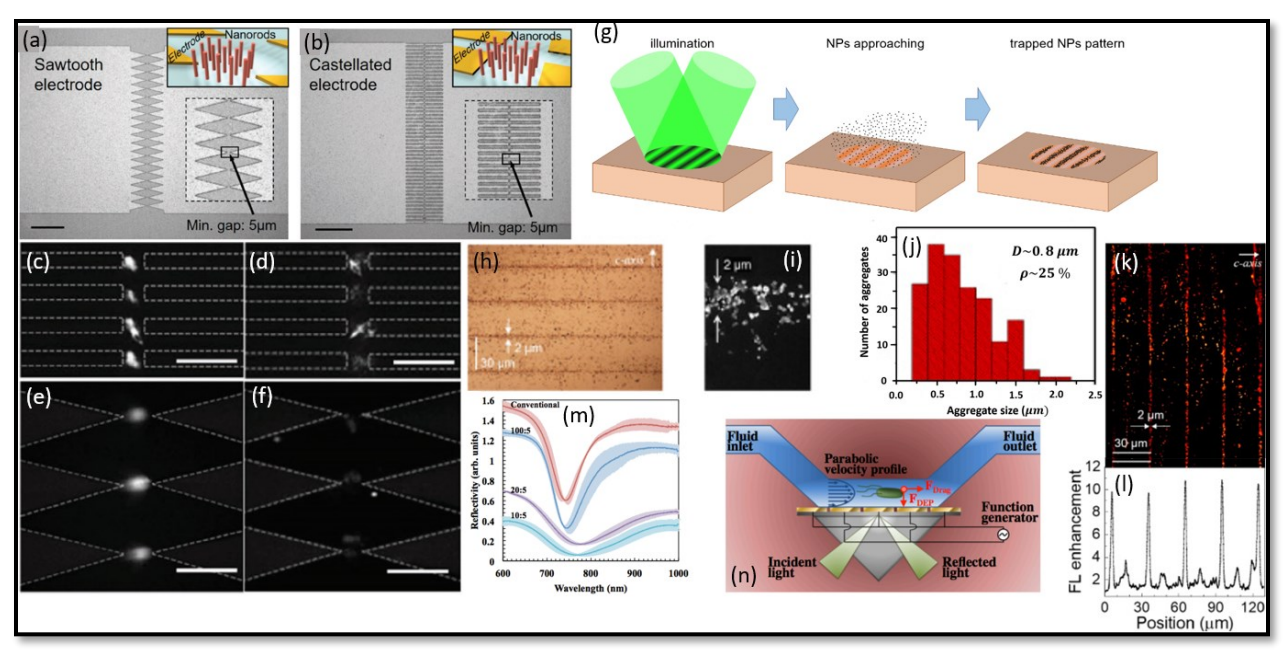


Fig. 7: Illustration of two types of electrode arrays used in the experiments: (a) sawtooth and (b) castellated electrode array, where the insets provide schematic representations of microelectrodes integrated with nanorods (NDs). Scale bars: 200 μm. Fluorescent images demonstrate the DEP behavior of bovine serum albumin (BSA) in the castellated electrode device at (c) 5Vp-p, 1MHz and (d) 5Vp-p, 10MHz, as well as the sawtooth electrode device at (e) 5Vp-p, 1MHz and (f) 5Vp-p, 10MHz, both incorporating oxide nanorods (NDs). (g) PVOT operation scheme using the sequential method involving sinusoidal light profile illumination on a z-cut PV substrate. (h) Microphotographs, (i) SEM images, and (j) histograms of fringes patterns (Pattern III) cluster sizes. (k) FL images and corresponding averages, (l) FL enhancement profiles along the perpendicular direction to the fringes for three Au 170 nm fringe patterns. (m) Contrast the reflectivity of conventional chips with iSPR chips (EG = 5.5 μm). IDEs are perpendicular to SP propagation for EW values of 10 μm, 20 μm, and 100 μm. (n) The DEP-SPR device employs DEP-active interdigitated electrodes (IDEs), replacing the traditional Au sensing surface in the Kretschmann SPR setup. Alternating IDEs, connected to a function generator, generate an AC potential for DEP, enabling the transportation of bacterial mass to the IDE sensing surface by overcoming fluid drag. Figures 7(a-f), (g-l) and (m, n) extracted with explicit permission from [141], [142] and [152], respectively.

A study reported by Zhen Cao et al. explored the integration of insulator-based dielectrophoresis (iDEP) with nanostructured sawtooth and castellated electrode arrays with the nanorods (NDs) for protein enrichment and the development of highly sensitive immunoassays (Fig 7: (a, b)) [141]. The authors described the fabrication process of the devices, which involves the deposition of SiO2 and Ag NDs using a customized e-beam evaporator. The ND arrays were designed to create a strong electric field and a high electric field gradient needed to efficiently enrich proteins. This study highlighted the effectiveness of the DEP integrated with ND arrays for protein binding and enrichment. The authors demonstrated a significant acceleration of binding kinetics through fast DEP trapping near the NDs, leading to a shorter incubation time compared to traditional methods [141]. The signal level reached a steady state within a minute, enabling fast detection of biomarkers. The validation of the concept was carried out using fluorescence-labeled beads and BSA protein, and the corresponding results are presented in Figure 7: (c-f). The specificity of the detection was evaluated by employing streptavidin proteins as a negative control, which showed a significantly smaller fluorescent signal compared to the positive response of mouse IgG. The incorporation of repeated washing steps during the assay helped to reduce nonspecific binding and eliminated the false-negative results. The accuracy of the assay system was assessed by examining the recovery rate of spiked mouse IgG in human serum. The percent recovery rates fall within the acceptable range of 80% to 120%, indicating the high accuracy of the platform for immunoassays [141]. The authors also demonstrated the clinical utility of their device by detecting prostate-specific antigen (PSA) in human serum, achieving a detection limit of 2.6 ng/mL [141].

Iris Elvira et al. conducted a study on the fabrication of a novel device combining DEP and plasmonic-based detection for enhanced molecular detection. Authors employed DEP as a powerful technique for manipulating and trapping molecules, while harnessing the plasmonic properties of metallic nanostructures to enhance the detection sensitivity (Fig 7: (g)) [142]. The device fabrication process involved the assembly of gold nanoparticles (Au NPs) into periodic micro-patterns using photovoltaic optoelectronic tweezers (PVOT). Two different sizes of Au NPs, 170

nm and 3.5 nm, were utilized to explore their respective performance [142]. The Au patterns fabricated through PVOT exhibited high homogeneity at the microscale and controlled spatial distribution of aggregates with micrometric accuracy (Fig 7: (h-j)). The plasmonic response of the patterns was characterized by reflectance spectroscopy, revealing broad plasmonic bands extending into the visible and near-infrared range. For fluorescence enhancement, the patterns were tested with molecules such as Rhodamine B (RB) dye and DNA biomolecules tagged with RB. The results demonstrated significant fluorescence enhancement factors, reaching up to 10-fold for RB dye and 3-fold for DNA biomolecules, when compared to control samples (Fig 7: (k, l)) [142]. This remarkable enhancement was attributed to the synergistic combination of DEP trapping and plasmonic effects, which led to increased excitation rates and quantum efficiencies of the molecules. The integration of DEP and plasmonic in the fabricated device showcases its potential for highly sensitive molecular detection. By leveraging the precise manipulation capabilities of DEP and the enhanced optical properties of plasmonic structures, the device offers a promising platform for various applications such as bio-imaging and biosensing. The fluorescence enhancement of DNA biomolecules tagged with RB further demonstrates the versatility of the device for molecular detection in biological systems.

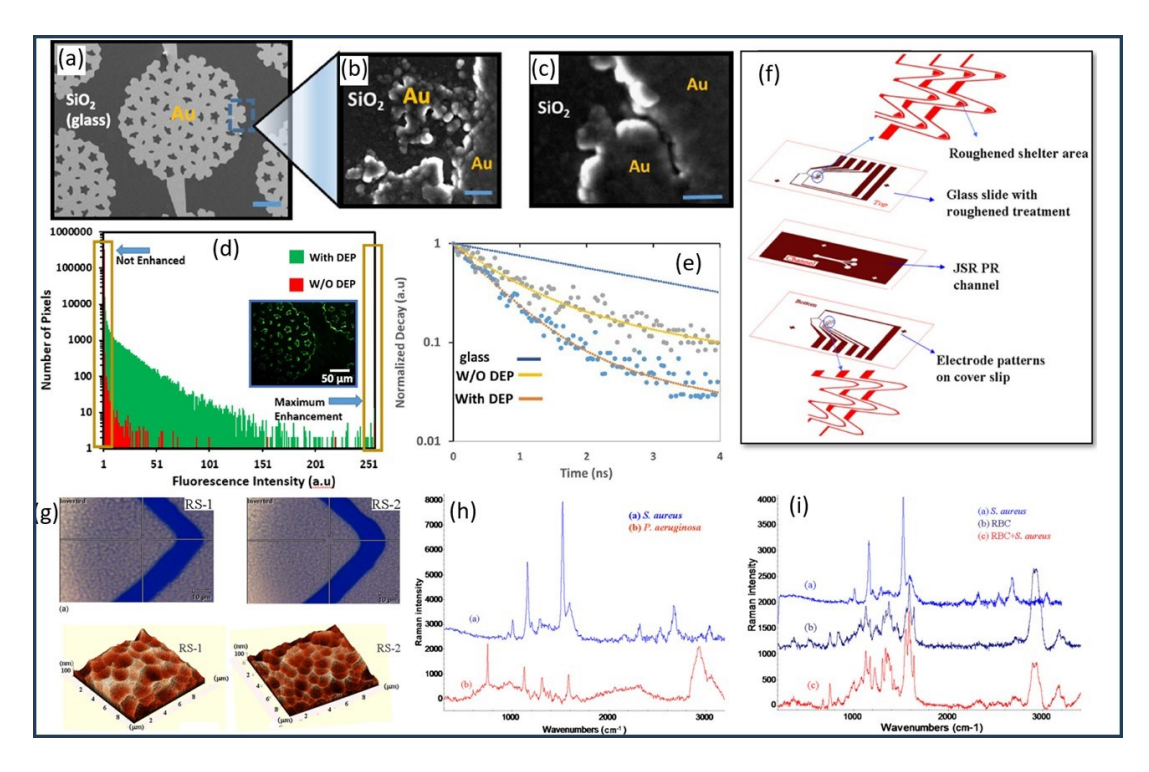


Fig. 8: (a) Fabrication and characterization of PIDEs and hotspots. (b) and (c) Characterization of the hotspots of various sizes and shapes using SEM. (d) Comparison of the fluorescence measured from a sample with and without DEP. The inset shows the picture of the sample with DEP used to generate the histogram plot. (e) Fluorescence decay curves for the TRITC labeled biotin molecules in glass coverslip, on electrodes with DEP and on electrodes without DEP. (f) Chip design and Construction. The chip design included bottom-layer electrodes on a cover slip and top-layer electrodes on treated glass. A metal shelter in front of the top-layer trapping electrode minimized fluorescence noise and boosted Raman signals. (g) Bright field microscope image (top) and Atomic Force Microscope (AFM) image (bottom) of two types of roughened Au surface. (h) The measurement results of S. aureus and P. aeruginosa show distinct SERS spectra that are promising for fingerprint discrimination. (i) SERS signatures of S. aureus, Red Blood Cells (RBC), and RBCs/bacteria mixture (RBCs: bacteria= 1: 10). Figures (a-e) have been extracted from [58], while figures (f-i) have been obtained from [145], all reused with explicit permission.

Velmanickam Logeeshan et al. presented a study on the integration of dielectrophoresis and fluorescence enhancement to enhance the detection of biomarker molecules using Pearl-shaped Interdigitated Electrodes (PIDEs) (Fig 8(a-c)) [58]. The study focused on the use of fluorescently labeled Avidin molecules as the target biomarkers, with the objective of quantifying low concentrations of Avidin using the integrated DEP and fluorescence enhancement. The authors employed PIDEs, which allows precise patterning and control of the electrode geometry.

The device fabrication technique ensures the formation of well-defined electrode structures, crucial for efficient DEP and fluorescence enhancement. To determine the optimum frequency of the electric field, the authors varied the frequency from 50 kHz to 500 kHz and measured the fluorescence intensity near the electrodes. Based on their results, a frequency of 120 kHz was identified as generating the highest fluorescence intensity, indicating efficient concentration of Avidin molecules in the hotspots [58]. The authors employed fluorescently labeled Avidin molecules with an excitation wavelength around 500 nm and an emission wavelength around 515 nm, enabling specific targeting and detection of the biomarkers [58]. Furthermore, the authors investigated the fluorescence decay curves of tetramethylrhodamine (TRITC) labeled streptavidin molecules using time-correlated single photon counting (TCSPC) to measure the fluorescence lifetime (Fig 8(e)). The results demonstrated a reduction in the fluorescence lifetime of molecules placed in the electrodes, providing evidence of the interaction between biomarkers and enhanced electric fields or surface plasmon polaritons (SPPs). The authors reported that their technique was capable of detecting about 1.5 pM of Avidin molecules [58]. This represents a significant improvement compared to the standard fluorescence technique, which could only detect Avidin at a concentration of 1.5 µM (Fig 8(d)). Therefore, the integrated technique enhances the detection of Avidin molecules by approximately 1,000,000-fold [58]. The research presented in this work reported an advancement in the field of biomarker detection by successfully integrating DEP and plasmonic effects. The novelty of this work lies in the fabrication of PIDEs using photolithography and their integration with fluorescence enhancement, enabling efficient concentration of biomarkers and their subsequent interaction with enhanced electric fields. The improvement in detection sensitivity, coupled with the remarkable detection limit improvement, highlights the potential of this integrated approach for the sensitive detection and quantification of biomarker molecules.

The integration of DEP force and surface-enhanced Raman scattering (SERS) offers several advantages, including rapid and sensitive analysis, label-free detection, and the ability to monitor molecules in real-time. Akinobu Yamaguchi et al. reported a technique for the detection of biomarkers at low concentrations by integrating dielectrophoretic manipulation and SERS [143]. This platform enables label-free, real-time monitoring of molecules with exceptional sensitivity. The fabrication of the electrode involves the use of gold electrodes and the manipulation of gold/polystyrene (Au/PS) microparticles. By applying an AC electric field at a frequency of 100 kHz, the attractive van der Waals forces between the Au/PS microparticles were utilized to aggregate and fix them at the middle of the gold electrodes [143]. This controlled aggregation creates unique "hot spots" that greatly enhance the SERS signal, allowing for highly sensitive detection of biomarkers. The researchers demonstrated the effectiveness of their platform by detecting and analyzing the Raman spectra of 4,4'-bipyridine (4bpy), a biomarker, in real-time. Notably, they achieved detection at concentrations as low as 100 pM, highlighting the exceptional sensitivity of their platform [143]. The fabrication techniques employed in this platform ensure the formation of a tight-knit higher-order structure consisting of the Au/PS microparticles and the biomarker, leading to accurate and reliable detection. This platform holds a promise for various applications, including biomarker detection, environmental pollutant analysis, and investigations of chemical and biological reactions, and opens avenues for its commercial utilization in "lab-on-a-chip" applications and the study of mammalian and plant cell cultures.

Giulia Barzan et al. developed a rapid antibiotic susceptibility test (AST) using a DEP-Raman device to obtain quick results in clinical and microbiological samples. The DEP-Raman device was fabricated using laser lithography, which allows for the creation of intricate and tailored structures with high resolution. The device enabled the characterization of various bacterial strains with high specificity and provided insights into dynamic bacterial interactions with antibiotics. By employing multivariate data analysis, the researchers modeled molecular-level spectral differences within just one hour of antibiotic treatment [144]. The Raman-based susceptibility test accurately classified bacteria as non-susceptible when treated with sub-minimal inhibitory concentration (MIC) levels of the antibiotic ciprofloxacin (CP), as well as bacteria displaying induced tolerance to the antibiotic due to pre-treatment with triclosan (TCS). Additionally, an environmental E. coli strain naturally resistant to CP was successfully identified as non-susceptible after only one hour of treatment at the minimum bactericidal concentration (MBC) of CP [144]. These findings underscore the remarkable potential of the DEP-Raman approach as a rapid and reliable method for AST, eliminating the laborious sample preparation and overnight incubation required by conventional microbiological techniques while offering high accuracy and versatility for various applications. The Raman-based susceptibility test exhibited promising performance in predicting bacterial susceptibility to antibiotics. The validation results showed that after 1 hour of treatment, the sensitivity in predicting susceptibility was 67%, which increased to 100% at 2 hours [144]. This result indicates that the DEP-Raman method successfully identified non-susceptible bacteria after a relatively short treatment duration. On the other hand, the specificity of the prediction was 100% after 1 hour but decreased to 50% and 33% at 2 hours and 3 hours, respectively. The classification error in the prediction was 17% at 1 hour, which rose to 25% and 33% at 2 hours and 3 hours,

respectively [144]. The combined DEP-Raman approach was further validated by standard microbiological assays, which confirmed the significant induction of tolerance over multiple time points after treatment. This method holds great promise for revolutionizing bacterial AST, eliminating the need for time-consuming sample preparation and overnight incubation required by traditional microbiological techniques. With its exceptional accuracy, versatility, and ability to provide rapid results, this approach has the potential to significantly improve patient outcomes and reduce the selection of antibiotic-resistant organisms.

I-Fang Cheng et al. developed a DEP-based microfluidic chip with a roughened metal surface for on-chip SERS detection of bacteria (Fig 8: (f)). The chip employed a laser power of approximately 1 mW for SERS signal collection from Staphylococcus aureus (S. aureus) [145]. Comparing smooth and roughened electrode surfaces, the researchers observed a significant 30-fold enhancement in the SERS signal due to the greater sharpness and higher electromagnetic tip enhancement provided by the roughened surface. The microfabrication process involved etching glass slides using buffered oxide etchant (BOE) solution to create surface roughness. Two types of roughened surfaces were obtained using controlled etching rates (Fig 8: (g)). After surface roughening, a thin Au/Cr layer was deposited on the glass slide and cover slip. Microelectrode patterning and photolithography techniques were employed to create a microchannel for sample flow. The chip demonstrated effective discrimination between Grampositive S. aureus and Gram-negative Pseudomonas aeruginosa (P. aeruginosa) bacteria in the detected SERS spectra (Fig 8: (h)). The study focused on the detection and concentration of bacteria using negative DEP force. The DEP behaviors of human red blood cells (RBCs) and S. aureus bacteria were observed to transition from negative to positive as the frequency increased beyond their respective crossover frequencies, which were approximately 700-800 kHz for RBCs and 6-7 MHz for S. aureus (Fig 8: (i)) [145]. The researchers prepared the sample by diluting the blood cell solution 1000-fold and resuspending it in an isotonic solution to achieve a final concentration of 106 cells/ml. Similarly, the bacterial solution was prepared at a concentration of 10<sup>6</sup> colony-forming units per milliliter (CFU/ml) [145]. These solutions were mixed in a 1:1 ratio to create the final mixture solution used in the study.

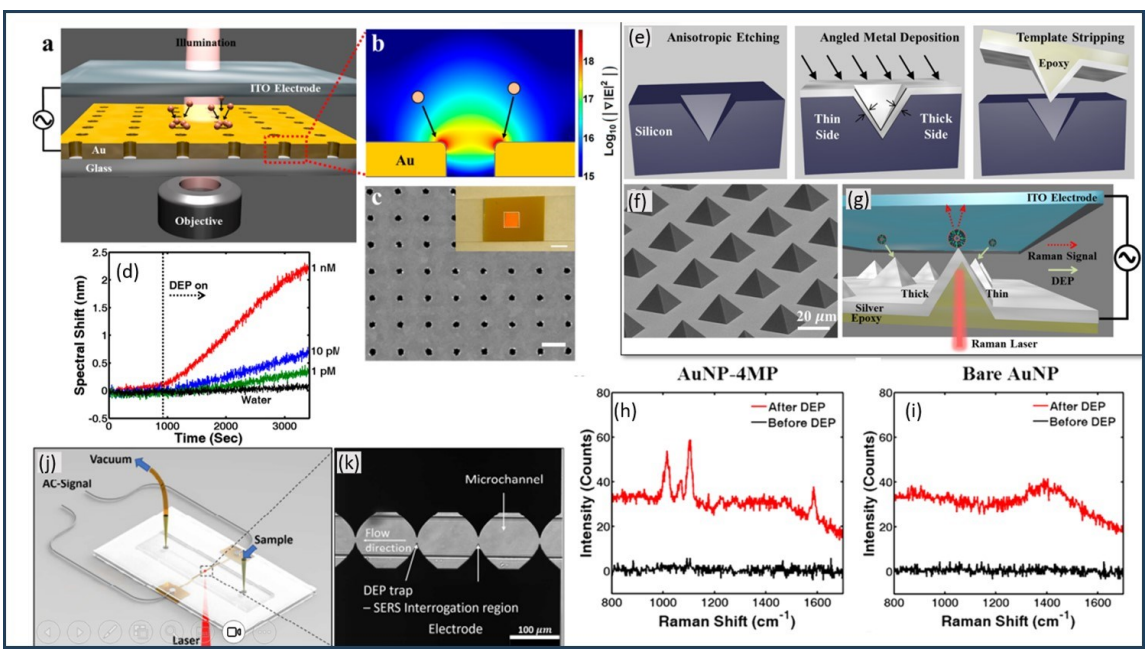


Fig. 9: (a) Schematic presentation of the experimental setup for used dielectrophoretic concentration of analyte molecules. (b) Dielectrophoretic forces pull analyte molecules toward hole edges where the electric field intensity gradient is strongest (red color). (c) SEM of a nanohole array reveals a ~140 nm hole diameter and 600 nm periodicity. Scale bar: 500 nm. Inset: Photo of the template-stripped gold nanohole array. Scale bar: 1 cm. (d) Detection of Low-concentration BSA. Also shows the time-resolved spectral shift from various concentrations of BSA (1 nM, 10 pM, and 1 pM) and control experiment (water). (e) Schematic representation of the template-stripping method used to fabricate an asymmetric pyramid array. (f) SEM image of template-stripped asymmetric pyramids with the base dimension of 20 μm ×20 μm. (g) Illustration of the experimental setup. (h) Raman signal collected before and after DEP trapping of AuNP-4MP on the tip of the pyramid. (i) Negative control experiment with bare AuNP showing disappearance of characteristic Raman peaks from 4MP. (j) PDMS microchannel is sandwiched between an electrode substrate and a glass cover. Yellow pipette tips serve as fluidic reservoirs/connections. Aluminum wires, soldered to contact pads, establish electrical connections between the chip and the AC signal generator. (k) Zoomed in view of

the micro channel and the electrodes. Figures (a-d), (e-i) and (j,k) are extracted from [146], [148], and [149] respectively with explicit permission.

Avijit Barik et al. presented a study on the integration of gold nanohole arrays with a transparent electrode to demonstrate the enhanced surface plasmon resonance (SPR) sensing using dielectrophoresis (Fig 9: (a-c)). In contrast to the suspended flow-through nanohole structure, the authors opt for dead-ended nanohole films, which offer easier fabrication and handling while still generating strong DEP forces for efficient molecular trapping [146]. By modulating the frequency of the applied alternating current (ac) signal, the authors successfully captured and released 190 nm polystyrene beads on the gold nanohole surface, showcasing the enhanced molecular transport [146]. Additionally, the biosensor achieves the detection of bovine serum albumin (BSA) molecules at a remarkable concentration of 1 pM in a 5 µL sample droplet (Fig 9: (d)) [146]. The experimental setup involves large-area gold nanohole arrays prepared through a combination of nanoimprinting and template stripping techniques. Transparent top electrodes composed of ITO-coated glass slides are utilized, and the gap between the ITO-coated slide and the gold nanohole array is defined using 3M Scotch Magic tape as a spacer [146]. Real-time monitoring of binding events is achieved by tracking the SPR wavelengths in the transmission spectrum. The nanohole array, characterized by a hole diameter of approximately 140 nm and a periodicity of 600 nm, exhibits resonant peaks and dips in the transmission spectrum indicative of SPR [146]. The spectral features shift towards longer wavelengths as the interfacial refractive index increases due to surface-bound molecules. To measure the resonance shift, a tungstenhalogen lamp illuminates the nanohole array, and the transmitted light is collected and analyzed using an imaging spectrometer coupled with a CCD camera. The study also demonstrates the manipulation of fluorescent polystyrene beads using dielectrophoresis. The absence of applied bias established a baseline measurement, while the application of positive DEP at 1 kHz and negative DEP at 10 MHz provided insights into the behavior of the system under different conditions. Voltage (10 Vp-p) and the specified frequencies ensured effective manipulation of the fluorescent polystyrene beads and enabled the researchers to study their response to the DEP forces [146]. The fluorescence measurements over the nanohole region reveal an increase in intensity during the positive DEP cycle, indicating successful molecular trapping, while a residual response persists during the subsequent negative DEP cycle due to suspended beads in proximity to the nanoholes.

On another study, Velmanickam Logeeshan et al. investigated an approach for augmenting the Radiative Decay Rate (RDR) of fluorophore molecules, specifically concentrating on Cy3-labeled miRNA-DNA duplexes [147]. The utility of external electric fields in this context could lead to significant advancements in the realm of fluorescence enhancement and biomolecular detection. The miRNA-DNA duplex molecules were labeled with the low quantum yield fluorophore Cy3 (Quantum yield: 0.04, excitation: 550 nm, emission: 570 nm) and probed how their lifetimes were affected when concentrated in hotspots using dielectrophoresis [147]. The T-shaped Interdigitated Array of Microelectrodes (TIAMs) in conjunction with fractal-like hotspots was used for these experiments. These intricate structures, which are created using a cost-effective method that rivals the traditional E-beam lithography technique, are critical for the successful integration of miRNA-DNA and subsequent fluorescence enhancement. The DEP force was used to concentrate the molecules inside the hotspots to enhance the fluorescence emission (Fig 6: (a-c)). The authors provided a detailed experimental protocol that employs low-quantum yield Cy3 fluorophore molecules and utilizes electric fields to modulate the RDR [147]. Their approach yields evidence for the possibility of RDR enhancement by employing an applied electric field, with the fluorophore's lifetime dropping from 1.92 ns (without hotspots or electric fields) to 0.35 ns when a 1MHz, 10 Vpp electric field is applied [147].

On another study, Avijit Barik et al. presented a study on the integration of Raman spectroscopy and Dielectrophoresis for label-free detection of analyte molecules loaded within small vesicles [148]. The authors emphasized the fabrication technique involving producing a large array of metallic pyramids for DEP-assisted Raman spectroscopy. The fabrication involves the use of standard (100) silicon wafers coated with a 100 nm thick Si<sub>3</sub>N<sub>4</sub> film, followed by photolithography and reactive ion etching to create circular holes of 20 µm diameter. This fabrication method yields approximately 100,000 pyramids on a 4-inch silicon wafer (Fig 9: (e-g)) [148]. These pyramids possess an asymmetrical metal thickness on opposite facets, creating subwavelength hotspots at the tip when illuminated with linearly polarized light. Through the combination of DEP preconcentration and nano focusing capabilities, the platform enables fast and directed transport of analytes [148]. The authors successfully trapped 200 nm vesicles and 70 nm gold nanoparticles, highlighting the potential for lab-on-a-chip devices used in studying subcellular structures [148]. To demonstrate label-free detection using Raman spectroscopy, gold nanoparticles coated with 4MP molecules (AuNP-4MP) are chosen as target particles. The DEP trapping of AuNP-4MP on the pyramid tips is achieved by applying a voltage of 8 Vpp at a frequency of 1 kHz (Fig 9: (h, i))[148]. The Raman signal is simultaneously collected, resulting in the appearance of signature Raman peaks from 4MP molecules. The

Raman peaks at 1013, 1065, 1099, and 1584  $cm^{-1}$  correspond to the ring-breathing mode, the in-plane C-H bend, the ring-breathing mode coupled with the v(C-S) stretching mode, and the ring-stretching mode, respectively [148]. The platform demonstrates an order of  $10^4$  enhancement in Raman scattering signals when the pyramid is internally illuminated. The platform is further used to detect the contents of vesicles through DEP-assisted Raman spectroscopy. Vesicles containing 4MP molecules are prepared, and an 8 Vpp potential at a frequency of 1 kHz is applied for trapping [148]. Real-time Raman signals are collected, showing the detection of 4MP molecules over time. Within 60 seconds of DEP, signal-to-noise ratios of 208 and 326 are observed at the Raman peaks of 1013 and  $1099 \ cm^{-1}$ , respectively [148]. The experimental setup offers low background and high signal-to-noise ratios in a fast manner, making it suitable for various experiments.

Reza Salemmilani et al. presented an integrated microfluidic-dielectrophoresis and surface-enhanced Raman scattering (SERS) platform (Fig 9: (j, k)) for the rapid and specific detection of methamphetamine in saliva under 2 mins [149]. The authors successfully addressed challenges related to silver nanoparticle stability, interference from capping agents, and device fouling, resulting in a robust and reusable detection system. By establishing electrical connections and applying AC potentials at specific frequencies, the authors achieved the controlled nanoparticle trapping and agglomeration within the microfluidic device. The experimental setup involves loading 25 µl of saliva samples pre-mixed with freshly prepared iodide-modified silver nanoparticles into the microfluidic device. The flow rate is adjusted to approximately 5 µL/min, and the device is placed on a LabRam Aramis Raman microscope platform with a 633-nm laser as the excitation source [149]. A 50X objective lens focused the laser onto one of the four trap regions. The fluid flow was then stopped, and a 16Vpp, 2.5 MHz AC potential was applied to the electrodes. The SERS signal intensity increases over time, reaching a maximum intensity after approximately 2 minutes, demonstrating the successful agglomeration of nanoparticles by dielectrophoresis [149]. To ensure reusability of the device and minimize fouling, the authors employed passivation techniques such as functionalizing gold electrodes with polyethylene glycol (PEG) and using fluorinated polymers on wet surfaces. After data acquisition, flow was re-established at a higher rate of approximately 20 µL/min, and an AC potential of 12 MHz at 80 Vpp was applied to the electrodes. This combination of high flow rate and secondary electrokinetically-induced flow clears the agglomerated nanoparticles from the microchannels, preparing the device for a new detection run. The authors demonstrated the reusability of the device by performing three consecutive detection-clearance cycles with 500 nM methamphetamine-positive saliva samples and negative controls [149]. By combining controlled nanoparticle trapping, passivation techniques, and optimized detection-clearance cycles, the authors overcame challenges associated with nanoparticle stability and device fouling. The platform's ability to detect methamphetamine at physiologically relevant concentrations, its compatibility with complex biological samples like saliva, and its demonstrated reusability make it a promising tool for point-of-care diagnosis.

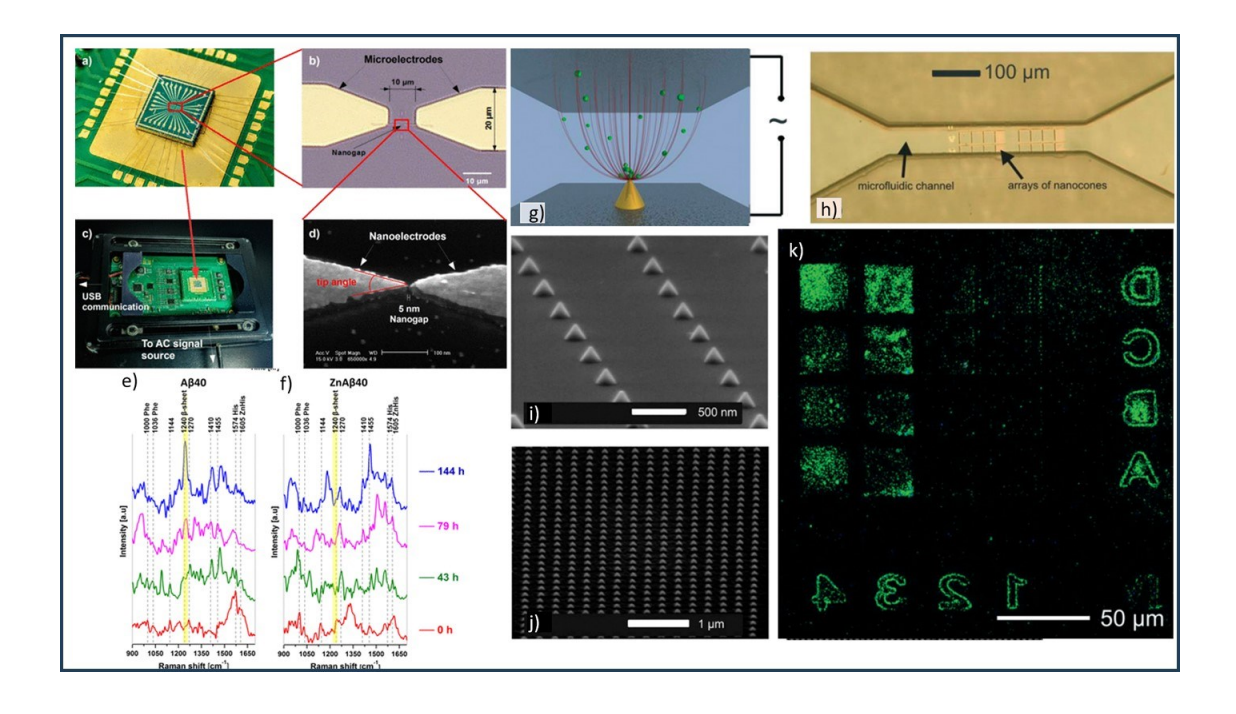


**Fig. 10:** (a)  $7 \times 7$  mm chip with wire-bonded connections featuring 15 pairs of gold (Au) electrodes. (b) Microscopic view of a single pair of microelectrodes and nanoelectrodes. (c) The sensing system integrated onto a specially designed printed circuit board. (d) Electron microscope image showcasing the nanogap between electrodes. Visualization of Aβ40 in solution using the ThT fluorescence assay. (e) SERS spectra captured by the nanogap device without Zn<sup>2+</sup>, and (f) with Zn<sup>2+</sup> at various time points (0, 43, 79, and 144 h). The highlighted yellow bars represent the amide III β-sheet mode at 1240 cm<sup>-1</sup>. Diagram showing particle capture by a metallic nano-cone through dielectrophoresis. (g) Indium Tin Oxide (ITO) electrode with a gold cone and a top ITO electrode connected to AC voltage. Particles in the solution (green) polarize and move along the squared electric field gradient (red lines). (h) Top view of gold nano-cone arrays in a microfluidic channel. SEM images of arrays of gold nano-cones with different cone distances: (i) 1 μm, (j) 500 nm. (k) Enhanced contrast fluorescence image depicts gold nano cones arranged in a fluidic channel following the capture of BSA molecules on the cone arrays through DEP. Figures were used with permission. (a-f) have been acquired from [151], and figures (g-k) were obtained from [152].

Christian Schäfer et al. presented study to introduce an approach for the targeted concentration and capture of biomarker molecules. Through the integration of gold nano-cones into microfluidic channels and the application of an alternating current (AC) voltage, the authors successfully demonstrated the efficient capture of bovine serum albumin (BSA) molecules [150]. The fabrication technique employed by Schäfer et al. involves the transfer of circular etch masks into a gold layer using argon ion milling, resulting in the formation of conical-shaped nanostructures (Fig 10 (g)-(j)). The nano-cones are then integrated into microfluidic channels using electron beam lithography and polymethyl methacrylate (PMMA) for the preparation of Al<sub>2</sub>O<sub>3</sub> etch masks [150]. This meticulous fabrication process ensures the precise positioning and alignment of the nano-cones within the fluidic channels, enabling effective molecule capture. The experimental results showcase the efficacy of the proposed method, with the collection of BSA molecules observed on the gold nano-cone arrays. The authors varied the channel height to optimize the electric field gradients, and for a channel height of 5 µm, a visibly increased concentration of fluorescently labeled BSA was achieved. An AC voltage of 10 V with a frequency of 2.5 MHz was applied between the nano-cone substrate and the channel cover to produce DEP forces [150]. The combination of plasmonic nanostructures, microfluidic channels, and dielectrophoresis holds significant promise for molecular sensing applications. The authors suggest that this method can be coupled with optical sensing techniques such as surfaceenhanced Raman spectroscopy (SERS) or localized surface plasmon resonance (LSPR) sensing, enabling high sensitivity and spatial resolution [150]. Furthermore, the integration of plasmonic nanostructures into microfluidic channels opens doors to incorporating sorting mechanisms, overcoming challenges related to nonspecific binding of different molecules during the sensing process (Fig 10 (1)).

Katrin H.P. Vu et al. presented a platform that combines dielectrophoresis trapping with SERS for protein conformation studies [151]. The device fabrication involved e-beam lithography and e-gun evaporation with a subsequent lift-off process on a silicon substrate coated with a 1 µm SiO2 layer (Fig 10 (a)- (d)). The nanostructures, including microwires and nanoelectrodes, were precisely defined using UV lithography and e-beam writing, respectively. Scanning electron microscopy was employed to inspect the fabricated chips, confirming the quality and dimensions of each nanogap. In experiments, Aβ40 peptides and FAM-Aβ42 oligomers were used. Aβ40 peptides were synthesized using Fmoc N-(9-fluorenyl) methoxycarbonyl solid-phase chemistry, purified by reverse-phase high-performance liquid chromatography, and dissolved in Tris-HCl buffer [151]. The Aβ40 solutions were prepared in the presence or absence of Zn2+ ions to investigate their effects on peptide aggregation. FAM-Aβ42 oligomers, purchased from Biopeptide, were used for fluorescence observations [151]. Fluorescence microscopy was employed to acquire images using an inverted fluorescence microscope equipped with an LED lamp as the light source. A 100× oil-immersion objective and an EMCCD camera were used to observe the fluorescent signals. Raman spectra were obtained using a confocal Raman microscope with a 640 nm excitation laser. The laser power was controlled to deliver 1-2 mW to the samples, and a 100× air objective was used to focus the laser on the nanoelectrodes [151]. Raman measurements were taken at different stages of peptide aggregation, and the recorded wavenumber axis was calibrated using the Si phonon peak (Fig 10 (e, f). By controlling the molecular orientation through DEP trapping, the researchers achieved consistent and enhanced SERS spectra [151]. The high sensitivity of the device allowed for the detection of low peptide concentrations, which is particularly relevant for studying biomarkers in physiological fluids.

Daniel David Galvan and his team conducted a study to improve the performance of surface plasmon resonance (SPR)-based bacterial biosensors. These biosensors often face challenges due to the diffusion-limited mass transport of bacteria to the sensing surface [152]. To overcome this, the team developed a dielectrophoresis (DEP)-enhanced SPR system, modifying conventional SPR chips with micron-sized gaps to generate interdigitated electrodes (IDEs)

on interdigitated SPR (iSPR) chips (Figure 7(n)). The IDEs were patterned into a ~3 μm SU-8 film on a silicon wafer, with fixed electrode gaps of 5 μm and electrode widths of 10, 20, and 100 μm (Figure 7 (m))[152]. These were then integrated into 50 nm Au films to create iSPR chips. The fabrication process involved several steps, including the creation of a patterned self-assembled monolayer (SAM) of ODT on the SPR chips and an Au etching solution to remove unprotected regions of the Cr/Au film [152]. These IDEs produced asymmetrical electric fields that exerted an external force on individual bacterial cells, driving cellular adsorption on the IDE surface for detection. The team investigated the effect of externally applied DEP on the generation of surface plasmons and the influence of the imposed dielectrophoretic force on mass transfer of bacterial cells during SPR-based detection. The iSPR chips with 100 µm electrode widths were found to effectively support SPR, with sensitivity comparable to conventional SPR chips. The team modified the surfaces of these iSPR chips with mannose to target the FimH adhesin of Escherichia coli, thereby increasing cellular adhesion. Authors have achieved a limit of detection (LOD) of approximately  $3.0 \times 10^2$  CFU/mL E. coli on mannosylated iSPR chips under positive-DEP conditions [152]. This represents a nearly five orders of magnitude improvement compared to mannosylated conventional SPR chips without DEP. Furthermore, authors amplified the SPR responses and enabled selective detection using anti-E. coli polyclonal antibodies, demonstrating that dilute suspensions of target bacteria can be selectively detected in the presence of non-target bacteria with iSPR chips.

Table 1: Advanced Techniques Combining Dielectrophoresis (DEP) with Various Sensing Modalities for Biomolecular Detection

Technique Used	Electrode Design	Advantages	Molecules Detected	References
DEP+ Plasmonic enhancement	T-shaped Interdigitated Array of Microelectrodes (TIAMs) with nanoscale plasmonic hotspots	Rapid and sensitive miRNA detection for point-of-care applications; superior sensitivity compared to conventional methods	miRNA	Velmanick am Logeeshan et al. [111]
DEP+ Plasmonic enhancement	T-shaped Interdigitated Array of Microelectrodes (TIAMs) with nanoscale plasmonic hotspots	Amplification of fluorescence intensity using AC electric fields; potential for highly sensitive biosensors for clinical applications	miRNA	Velmanick am Logeeshan et al. [138]
Integration of plasmonic and electronics	Split-trench resonator platform	Integration of high-quality-factor resonant plasmonic biosensors with RF nanogap tweezers; dielectrophoretic trapping of analytes	Nanoparticles and proteins	Dehan Yoo et al. [140]
Integration of insulator-based dielectrophoresis (iDEP)	Nanostructured sawtooth and castellated electrode arrays with nanorods (NDs)	Protein enrichment and development of highly sensitive immunoassays; fast DEP trapping near the NDs accelerates binding kinetics	Fluorescence- labeled beads, BSA protein, PSA in human serum	Zhen Cao et al. [141]
DEP and plasmonic-based detection	Assembly of gold nanoparticles (Au NPs) into periodic micro-patterns using photovoltaic optoelectronic tweezers (PVOT)	Manipulating and trapping molecules with DEP while enhancing detection sensitivity with plasmonic properties of metallic nanostructures	Rhodamine B dye, DNA biomolecules	Iris Elvira et al. [142]
Integration of DEP and fluorescence enhancement	Pearl-shaped Interdigitated Electrodes (PIDEs)	Enhancement of biomarker molecule detection by integrating DEP and fluorescence enhancement; precise patterning and control of electrode geometry	Avidin molecules	Velmanick am Logeeshan et al. [58]
Integration of DEP force and surface-enhanced Raman scattering (SERS)	Gold electrodes and gold/polystyrene (Au/PS) microparticles	Rapid and sensitive analysis, label-free detection, real-time monitoring of molecules; controlled aggregation creates unique "hot spots" for highly sensitive detection	4,4'-bipyridine (4bpy) biomarker	Akinobu Yamaguchi et al. [143]

DEP-Raman device for rapid antibiotic susceptibility testing	Fabricated using laser lithography	Rapid antibiotic susceptibility testing; high resolution and specificity for characterizing bacterial strains	Various bacterial strains	Giulia Barzan et al. [144]
DEP-based microfluidic chip with roughened metal surface for on-chip SERS detection of bacteria	Roughened metal surface	Effective discrimination between Gram-positive and Gram-negative bacteria using SERS; significant enhancement in SERS signal due to surface roughness	Bacteria	I-Fang Cheng et al. [145]
Enhanced surface plasmon resonance (SPR) sensing using DEP	Gold nanohole arrays with transparent electrode	Enhanced SPR sensing by integrating gold nanohole arrays with transparent electrode using DEP; easier fabrication and handling with dead-ended nanohole films	Bovine serum albumin (BSA) molecules	Avijit Barik et al. [146]
Targeted concentration and capture of biomarker molecules	Integration of gold nano- cones into microfluidic channels	Efficient capture of BSA molecules through integration of gold nano-cones and application of AC voltage; promising for molecular sensing applications	Bovine serum albumin (BSA) molecules	Christian Schäfer et al. [150]
DEP trapping combined with SERS for protein conformation studies	Microwires and nanoelectrodes fabricated using e-beam lithography and e-gun evaporation	Control of molecular orientation through DEP trapping for consistent and enhanced SERS spectra; high sensitivity for detection of low peptide concentrations	Aβ40 peptides and FAM- Aβ42 oligomers	Katrin H.P. Vu et al. [151]
Integrated microfluidic- dielectrophoresis and surface- enhanced Raman scattering (SERS) platform	Microfluidic device with silver nanoparticles and passivation techniques	Rapid and specific detection of methamphetamine in saliva under 2 minutes; overcoming challenges associated with nanoparticle stability and device fouling	Methamphetam ine in saliva	Reza Salemmila ni et al. [149]
Dielectrophoresis- induced plasmonic enhancement	T-shaped Interdigitated Array of Microelectrodes (TIAMs) with nanoscale plasmonic hotspots	Augmentation of Radiative Decay Rate (RDR) of fluorophore molecules using DEP; significant fluorescence enhancement and potential for biomolecular detection	Cy3-labeled miRNA-DNA duplexes	Velmanick am Logeeshan et al. [147]

### F. Conclusions

We discussed the recent efforts of integrated electric fields and optical detection techniques toward the detection of biomarkers. Fluorescence spectroscopy is one of the widely utilized techniques in biomarker detection. Since fluorescence enhancement play a critical role in detection of weak fluorescence, deep understanding of how each fundamental mechanism exclusively contributes to the fluorescence enhancement is needed to successfully enhance the fluorescence beyond current capabilities. Since all three of the mechanisms are directly related to near-field electromagnetic phenomena, their contribution to fluorescence enhancement is primarily dependent on the metal-fluorophore distance and their orientation [49],[58],[62],[64],[70]. We have discussed the utility of low frequency electric fields (< 5MHz) and DEP force to integrate and optimize the near-field electromagnetic phenomena. Additional investigations are needed for enhance the deep understanding of metal-fluorophore interactions using low electric fields and DEP force. In addition, studies have used the DEP force to separate molecules, e.g., isolate fluorophore-labeled miRNA-DNA duplexes without contamination with non-hybridized fluorophore labeled

complementary DNA molecules in hotspots. Utilizing dielectrophoresis successfully requires fundamental understanding on the electric polarization of biomarker molecules [132]. Dielectrophoresis studies have also focused on studying the long nucleic acid molecules (e.g., mRNA and DNA) and proteins. Unfortunately, the basic understanding of short nucleic acid molecules is still developing, especially for short miRNA, DNA and miRNA-DNA duplex molecules [111],[136]. Therefore, future studies should focus on estimating the frequency dependent electric polarization of miRNA, short DNA, miRNA-DNA duplexes, antigens, and antigen-antibody molecules. These studies will provide new knowledge on how molecular structures (single and double stranded) and types of molecules (miRNA and DNA) interact with electric fields and polarize in a frequency-dependent manner. Overall, based on our review of recent published studies, integrated optical detection and electric fields show a great promise toward detecting biomarkers in clinical samples at point-of-care. We believe that the combination of electric fields and optical detection provides a viable pathway for rapid and sensitive detection of biomarkers at point-of-care. Once fully developed, rapid biomarker detection can be performed at point-of-care eighter to develop diagnostic and prognostics tests or to develop routine screening for cancer and other diseases.

## Acknowledgment

DN acknowledges the financial support from the National Science Foundation (grant numbers: 2300064 and 2310106).

#### **References:**

- (1) American Cancer Society, A. Global Cancer: Facts & Figures. *Society* **2008**. https://doi.org/10.1002/ijc.27711.
- Wang, Y. C.; McPherson, K.; Marsh, T.; Gortmaker, S. L.; Brown, M. Health and Economic Burden of the Projected Obesity Trends in the USA and the UK. *Lancet* **2011**. https://doi.org/10.1016/S0140-6736(11)60814-3.
- (3) Birnbaum, H. G.; White, A. G.; Schiller, M.; Waldman, T.; Cleveland, J. M.; Roland, C. L. Societal Costs of Prescription Opioid Abuse, Dependence, and Misuse in the United States. *Pain Med.* **2011**. https://doi.org/10.1111/j.1526-4637.2011.01075.x.
- (4) Florence, C. S.; Zhou, C.; Luo, F.; Xu, L. The Economic Burden of Prescription Opioid Overdose, Abuse, and Dependence in the United States, 2013. *Med. Care* **2016**. https://doi.org/10.1097/MLR.00000000000000525.
- (5) Hayba, N.; Partridge, S. R.; Nour, M. M.; Grech, A.; Allman Farinelli, M. Effectiveness of Lifestyle Interventions for Preventing Harmful Weight Gain among Young Adults from Lower Socioeconomic Status and Ethnically Diverse Backgrounds: A Systematic Review. *Obesity Reviews*. 2018. https://doi.org/10.1111/obr.12641.
- (6) Poruk, K. E.; Firpo, M. a; Adler, D. G.; Mulvihill, S. J. Screening for Pancreatic Cancer: Why, How, and Who? *Ann Surg* **2013**, *257* (1), 17–26. https://doi.org/10.1097/SLA.0b013e31825ffbfb.Screening.
- (7) McGraw, C. Why Heroin Relapse Rate Is So High http://www.theclearingnw.com/blog/why-heroin-relapse-rate-is-so-high. https://doi.org/10.1360/zd-2013-43-6-1064.
- (8) E.B., P.; D.M., C.; L.M., B.; S.M., P.; V.G., C.; Hawley, J. A. Circulating Microrna Responses between "high" and "Low" Responders to a 16-Wk Diet and Exercise Weight Loss Intervention. *PLoS One* **2016**.
- (9) Chalana, H.; Kundal, T.; Gupta, V.; Malhari, A. S. Predictors of Relapse after Inpatient Opioid Detoxification during 1-Year Follow-Up. *J. Addict.* **2016**. https://doi.org/10.1155/2016/7620860.
- (10) Ji, D. L.; Li, C. L.; Cui, Y. F. Early Diagnosis of Pancreatic Cancer. *World Chinese J. Dig.* **2014**, *22* (17), 2406–2413. https://doi.org/10.11569/wcjd.v22.i17.2406.
- (11) Goonetilleke, K. S.; Siriwardena, A. K. Systematic Review of Carbohydrate Antigen (CA 19-9) as a Biochemical Marker in the Diagnosis of Pancreatic Cancer. *European Journal of Surgical Oncology*. 2007. https://doi.org/10.1016/j.ejso.2006.10.004.
- (12) Ganepola, G. A.; Rutledge, J. R.; Suman, P.; Yiengpruksawan, A.; Chang, D. H. Novel Blood-Based MicroRNA Biomarker Panel for Early Diagnosis of Pancreatic Cancer. *World J Gastrointest Oncol January* **2014**. https://doi.org/10.4251/wjgo.v6.i1.22.
- (13) Understanding the Epidemic Understanding the Epidemic.
- (14) Toyama, K.; Kiyosawa, N.; Watanabe, K.; Ishizuka, H. Identification of Circulating MiRNAs Differentially

- Regulated by Opioid Treatment. Int. J. Mol. Sci. 2017. https://doi.org/10.3390/ijms18091991.
- (15) Wu, Q.; Zhang, L.; Law, P.-Y.; Wei, L.-N.; Loh, H. H. Long-Term Morphine Treatment Decreases the Association of -Opioid Receptor (MOR1) MRNA with Polysomes through MiRNA23b. *Mol. Pharmacol.* **2009**. https://doi.org/10.1124/mol.108.053462.
- (16) Wu, Q.; Hwang, C. K.; Zheng, H.; Wagley, Y.; Lin, H. Y.; Kim, D. K.; Law, P. Y.; Loh, H. H.; Wei, L. N. MicroRNA 339 Down-Regulates μ-Opioid Meceptor at the Post-Transcriptional Level in Response to Opioid Treatment. *FASEB J.* 2013. https://doi.org/10.1096/fj.12-213439.
- (17) Barbierato, M.; Zusso, M.; Skaper, S.; Giusti, P. MicroRNAs: Emerging Role in the Endogenous μ Opioid System. *CNS Neurol. Disord. Drug Targets* **2015**, *14* (2), 239–250. https://doi.org/10.2174/1871527314666150116123932.
- (18) WEIGHT LOSS SURGERY INSURANCE COVERAGE AND COSTS https://www.obesitycoverage.com/weight-loss-surgery-insurance-coverage-and-costs/.
- (19) Völgyi, E.; Tylavsky, F. A.; Lyytikäinen, A.; Suominen, H.; Alén, M.; Cheng, S. Assessing Body Composition with DXA and Bioimpedance: Effects of Obesity, Physical Activity, and Age. *Obesity* **2008**. https://doi.org/10.1038/oby.2007.94.
- (20) Miller, W. C.; Koceja, D. M.; Hamilton, E. J. A Meta-Analysis of the Past 25 Years of Weight Loss Research Using Diet, Exercise or Diet plus Exercise Intervention. *Int. J. Obes.* **1997**. https://doi.org/10.1038/sj.ijo.0800499.
- (21) K.M., G.; K.A., L.; G.C., B.; P.D., G.; M.A., H. Epigenetic Mechanisms and the Mismatch Concept of the Developmental Origins of Health and Disease. *Pediatr. Res.* **2007**. https://doi.org/10.1203/pdr.0b013e318045bedb LK http://sfx.library.uu.nl/utrecht?sid=EMBASE&issn=00313998&id=doi:10.1203%2Fpdr.0b013e318045bedb &atitle=Epigenetic+mechanisms+and+the+mismatch+concept+of+the+developmental+origins+of+health+a nd+disease&stitle=Pediatr.+Res.&title=Pediatric+Research&volume=61&issue=5+PART+2+SUPPL.&spa ge=&epage=&aulast=Godfrey&aufirst=Keith+M.&auinit=K.M.&aufull=Godfrey+K.M.&coden=PEREB&i sbn=&pages=-&date=2007&auinit1=K&auinitm=M.
- (22) Hanson, M.; Godfrey, K. M.; Lillycrop, K. A.; Burdge, G. C.; Gluckman, P. D. Developmental Plasticity and Developmental Origins of Non-Communicable Disease: Theoretical Considerations and Epigenetic Mechanisms. *Progress in Biophysics and Molecular Biology*. 2011. https://doi.org/10.1016/j.pbiomolbio.2010.12.008.
- (23) Reinhard, S. The Thrifty Epigenotype: An Acquired and Heritable Predisposition for Obesity and Diabetes? *BioEssays* **2008**.
- (24) T., M.; J.M., C. DNA Methylation Biomarkers: Cancer and Beyond. *Genes (Basel)*. **2014**. https://doi.org/10.3390/genes5030821.
- (25) Tang, W. Y.; Ho, S. M. Epigenetic Reprogramming and Imprinting in Origins of Disease. *Reviews in Endocrine and Metabolic Disorders*. 2007. https://doi.org/10.1007/s11154-007-9042-4.
- (26) Mercer, T. R.; Mattick, J. S. Structure and Function of Long Noncoding RNAs in Epigenetic Regulation. *Nature Structural and Molecular Biology*. 2013. https://doi.org/10.1038/nsmb.2480.
- (27) Arroyo, J. D.; Chevillet, J. R.; Kroh, E. M.; Ruf, I. K.; Pritchard, C. C.; Gibson, D. F.; Mitchell, P. S.; Bennett, C. F.; Pogosova-Agadjanyan, E. L.; Stirewalt, D. L.; et al. Argonaute2 Complexes Carry a Population of Circulating MicroRNAs Independent of Vesicles in Human Plasma. *Proc. Natl. Acad. Sci.* **2011**, *108* (12), 5003–5008. https://doi.org/10.1073/pnas.1019055108.
- (28) Moldovan, L.; Batte, K. E.; Trgovcich, J.; Wisler, J.; Marsh, C. B.; Piper, M. Methodological Challenges in Utilizing MiRNAs as Circulating Biomarkers. *J. Cell. Mol. Med.* **2014**, *18* (3), 371–390. https://doi.org/10.1111/jcmm.12236.
- (29) Sohel, M. H. Extracellular/Circulating MicroRNAs: Release Mechanisms, Functions and Challenges. *Achiev. Life Sci.* **2016**, *10* (2), 175–186. https://doi.org/10.1016/j.als.2016.11.007.
- (30) S.L., M.; B.P., T.; A.L., P.; O., G.; Y., M.; S.F., N.; Mumford, S. L.; Towler, B. P.; Pashler, A. L.; Gilleard, O.; et al. Circulating MicroRNA Biomarkers in Melanoma: Tools and Challenges in Personalised Medicine. *Biomolecules* **2018**. https://doi.org/10.3390/biom8020021.
- (31) El-Khoury, V.; Pierson, S.; Kaoma, T.; Bernardin, F.; Berchem, G. Assessing Cellular and Circulating MiRNA Recovery: The Impact of the RNA Isolation Method and the Quantity of Input Material. *Sci. Rep.* **2016**, *6* (December 2015), 1–14. https://doi.org/10.1038/srep19529.
- (32) Roy, S.; Soh, J. H.; Gao, Z. A Microfluidic-Assisted Microarray for Ultrasensitive Detection of MiRNA under an Optical Microscope. *Lab Chip* **2011**. https://doi.org/10.1039/c0lc00638f.
- (33) S., K.; M.A., A.; P., A.; V.V., A.; R., J.; S., M. Microfluidic-Integrated Biosensors: Prospects for Point-of-

- Care Diagnostics. Biotechnology Journal. 2013.
- (34) Degliangeli, F.; Pompa, P. P.; Fiammengo, R. Nanotechnology-Based Strategies for the Detection and Quantification of MicroRNA. *Chemistry A European Journal*. 2014. https://doi.org/10.1002/chem.201402649.
- (35) Cheng, L.; Quek, C. Y. J.; Sun, X.; Bellingham, S. A.; Hill, A. F. The Detection of MicroRNA Associated with Alzheimer's Disease in Biological Fluids Using next-Generation Sequencing Technologies. *Front. Genet.* **2013**. https://doi.org/10.3389/fgene.2013.00150.
- (36) Pritchard, C. C.; Cheng, H. H.; Tewari, M.; Division, B.; Hutchinson, F.; Health, P.; Divisions, S.; Hutchinson, F. MicroRNA Profiling: Approaches and Considerations Colin. *Nat Rev Genet* **2015**, *13* (5), 358–369. https://doi.org/10.1038/nrg3198.MicroRNA.
- (37) Zubakov, D.; Boersma, A. W. M.; Choi, Y.; Van Kuijk, P. F.; Wiemer, E. A. C.; Kayser, M. MicroRNA Markers for Forensic Body Fluid Identification Obtained from Microarray Screening and Quantitative RT-PCR Confirmation. *Int. J. Legal Med.* 2010. https://doi.org/10.1007/s00414-009-0402-3.
- (38) Dong, H.; Lei, J.; Ding, L.; Wen, Y.; Ju, H.; Zhang, X. MicroRNA: Function, Detection, and Bioanalysis. *Chemical Reviews*. 2013. https://doi.org/10.1021/cr300362f.
- (39) Tiberio, P.; Callari, M.; Angeloni, V.; Daidone, M. G.; Appierto, V. Challenges in Using Circulating MiRNAs as Cancer Biomarkers. *Biomed Res. Int.* **2015**, 2015. https://doi.org/10.1155/2015/731479.
- (40) Tuck, M. K.; Chan, D. W.; Chia, D.; Godwin, A. K.; Grizzle, W. E.; Krueger, K. E.; Rom, W.; Sanda, M.; Sorbara, L.; Stass, S.; et al. Standard Operating Procedures for Serum and Plasma Collection: Early Detection Research Network Consensus Statement Standard Operating Procedure Integration Working Group. J. Proteome Res. 2009. https://doi.org/10.1021/pr800545q.
- (41) Teunissen, C. E.; Petzold, A.; Bennett, J. L.; Berven, F. S.; Brundin, L.; Comabella, M.; Franciotta, D.; Frederiksen, J. L.; Fleming, J. O.; Furlan, R.; et al. A Consensus Protocol for the Standardization of Cerebrospinal Fluid Collection and Biobanking. *Neurology*. 2009. https://doi.org/10.1212/WNL.0b013e3181c47cc2.
- (42) Sharma, A.; Schulman, S. G. *An Introduction to Fluorescence Spectroscopy*; 1999. https://doi.org/10.1016/S0026-265X(00)00048-5.
- (43) Gooijer, C. Introduction to Fluorescence Spectroscopy. *Anal. Chim. Acta* **2000**. https://doi.org/10.1016/S0003-2670(00)01086-2.
- (44) Sauer, M.; Hofkens, J.; Enderlein, J. Basic Principles of Fluorescence Spectroscopy. In *Handbook of Fluorescence Spectroscopy and Imaging: From Single Molecules to Ensebles*; 2011. https://doi.org/10.1385/0-89603-301-5:65.
- (45) Lakowicz, J. R.; Masters, B. R. Principles of Fluorescence Spectroscopy, Third Edition. *J. Biomed. Opt.* **2008**. https://doi.org/10.1117/1.2904580.
- (46) Rho, J. H. Fluorescence Spectroscopy. *Space Life Sciences*. 1972. https://doi.org/10.1007/BF00926765.
- (47) Steiner, R. F. Principles of Fluorescence Spectroscopy. Anal. Biochem. 1984. https://doi.org/10.1016/0003-2697(84)90125-8.
- (48) Lakowicz, J. R.; Malicka, J.; D'Auria, S.; Gryczynski, I. Release of the Self-Quenching of Fluorescence near Silver Metallic Surfaces. *Anal. Biochem.* **2003**. https://doi.org/10.1016/S0003-2697(03)00351-8.
- (49) Aslan, K.; Gryczynski, I.; Malicka, J.; Matveeva, E.; Lakowicz, J. R.; Geddes, C. D. Metal-Enhanced Fluorescence: An Emerging Tool in Biotechnology. *Current Opinion in Biotechnology*. 2005. https://doi.org/10.1016/j.copbio.2005.01.001.
- (50) Borisov, S. M.; Wolfbeis, O. S. Optical Biosensors. Chem. Rev. 2008. https://doi.org/10.1021/cr068105t.
- (51) Morales-Narváez, E.; Golmohammadi, H.; Naghdi, T.; Yousefi, H.; Kostiv, U.; Horák, D.; Pourreza, N.; Merkoçi, A. Nanopaper as an Optical Sensing Platform. ACS Nano 2015. https://doi.org/10.1021/acsnano.5b03097.
- (52) Shtenberg, G.; Segal, E. Porous Silicon Optical Biosensors. In *Handbook of Porous Silicon: Second Edition*; 2018; Vol. 2–2, pp 1263–1273. https://doi.org/10.1007/978-3-319-71381-6\_87.
- (53) Damborský, P.; Švitel, J.; Katrlík, J.; Dey, D.; Goswami, T.; Liedberg, B.; Nylander, C.; Lunström, I.; Schasfoort, R. B. M.; Tudos, A. J.; et al. Optical Biosensors. *Essays Biochem.* **2016**, *60* (1), 91–100. https://doi.org/10.1042/EBC20150010.
- Patel, P. N.; Mishra, V.; Mandloi, A. S. Optical Biosensors: Fundamentals & Trends. *J. Eng. Res. Stud.* **2010**, *I* (I), 15–34.
- (55) Carrara, S. *Nano-Bio-Sensing*; 2011. https://doi.org/10.1007/978-1-4419-6169-3.
- (56) Kim, D.; Daniel, W. L.; Mirkin, C. A. Microarray-Based Multiplexed Scanometric Immunoassay for Protein Cancer Markers Using Gold Nanoparticle Probes. *Anal. Chem.* **2009**. https://doi.org/10.1021/ac9018389.

- (57) Rusling, J. F.; Kumar, C. V.; Gutkind, J. S.; Patel, V. Measurement of Biomarker Proteins for Point-of-Care Early Detection and Monitoring of Cancer. *Analyst* **2010**. https://doi.org/10.1039/c0an00204f.
- Velmanickam, L.; Fondakowski, M.; Lima, I. T.; Nawarathna, D. Integrated Dielectrophoretic and Surface Plasmonic Platform for Million-Fold Improvement in the Detection of Fluorescent Events. *Biomicrofluidics* **2017**. https://doi.org/10.1063/1.5000008.
- (59) Fu, C. C.; Ossato, G.; Long, M.; Digman, M. A.; Gopinathan, A.; Lee, L. P.; Gratton, E.; Khine, M. Bimetallic Nanopetals for Thousand-Fold Fluorescence Enhancements. *Appl. Phys. Lett.* **2010**, *97* (20), 1–4. https://doi.org/10.1063/1.3495773.
- (60) White, I. M.; Yazdi, S. H.; Yu, W. W. Optofluidic SERS: Synergizing Photonics and Microfluidics for Chemical and Biological Analysis. *Microfluidics and Nanofluidics*. 2012. https://doi.org/10.1007/s10404-012-0962-2.
- (61) Dutta Choudhury, S.; Badugu, R.; Ray, K.; Lakowicz, J. R. Silver-Gold Nanocomposite Substrates for Metal-Enhanced Fluorescence: Ensemble and Single-Molecule Spectroscopic Studies. *J. Phys. Chem. C* 2012. https://doi.org/10.1021/jp212242x.
- (62) Lakowicz, J. R. Radiative Decay Engineering: Biophysical and Biomedical Applications. *Anal. Biochem.* **2001**, 298 (1), 1–24. https://doi.org/10.1006/abio.2001.5377.
- (63) Geddes, C. D.; Lakowicz, J. R. Editorial: Metal-Enhanced Fluorescence. *J. Fluoresc.* **2002**, *12* (2), 121–129. https://doi.org/10.1023/A:1016875709579.
- (64) Lakowicz, J. R. Radiative Decay Engineering 5: Metal-Enhanced Fluorescence and Plasmon Emission. *Anal. Biochem.* **2005**, *337* (2), 171–194. https://doi.org/10.1016/j.ab.2004.11.026.
- (65) Albani, J. R. Fluorescence Quenching. In *Structure and Dynamics of Macromolecules: Absorption and Fluorescence Studies*; 2004. https://doi.org/10.1016/B978-044451449-3/50004-6.
- (66) Dulkeith, E.; Morteani, A. C.; Niedereichholz, T.; Klar, T. A.; Feldmann, J.; Levi, S. A.; van Veggel, F. C. J. M.; Reinhoudt, D. N.; Möller, M.; Gittins, D. I. Fluorescence Quenching of Dye Molecules near Gold Nanoparticles: Radiative and Nonradiative Effects. *Phys. Rev. Lett.* 2002. https://doi.org/10.1103/PhysRevLett.89.203002.
- (67) Lakowicz, J. R. Quenching of Fluorescence. In *Principles of Fluorescence Spectroscopy*; 1983. https://doi.org/10.1007/978-1-4615-7658-7 9.
- (68) Geddes, C. D. Metal-Enhanced Fluorescence; 2010. https://doi.org/10.1002/9780470642795.
- (69) Gryczynski, I.; Malicka, J.; Gryczynski, Z.; Lakowicz, J. R. Radiative Decay Engineering 4. Experimental Studies of Surface Plasmon-Coupled Directional Emission. *Anal. Biochem.* **2004**, *324* (2), 170–182. https://doi.org/10.1016/j.ab.2003.09.036.
- (70) Geddes, C. D.; Lakowicz, J. R. Metal-Enhanced Fluorescence. In *Journal of Fluorescence*; 2002. https://doi.org/10.1023/A:1016875709579.
- (71) Velmanickam, L.; Chang, D. H.; Ganepola, G. A.; Nawarathna, D. Low-Cost and Rapid Micro-RNA Assay for Identification of Pancreactic Cancer. In 2021 IEEE Research and Applications of Photonics in Defense Conference, RAPID 2021; Institute of Electrical and Electronics Engineers Inc., 2021. https://doi.org/10.1109/RAPID51799.2021.9521412.
- (72) Pohl, H. A. The Motion and Precipitation of Suspensoids in Divergent Electric Fields. *J. Appl. Phys.* **1951**, 22 (7), 869–871. https://doi.org/10.1063/1.1700065.
- (73) Pethig, R. Publisher's Note: "Review Article-Dielectrophoresis: Status of the Theory, Technology, and Applications" [Biomicrofluidics 4, 022811 2010]. *Biomicrofluidics*. 2010. https://doi.org/10.1063/1.3474458.
- (74) Gupta, T. Dielectric Materials. In *Copper Interconnect Technology*; 2009. https://doi.org/10.1007/978-1-4419-0076-0 2.
- (75) Sihvola, A. Dielectric Polarization and Particle Shape Effects. *Journal of Nanomaterials*. 2007. https://doi.org/10.1155/2007/45090.
- (76) Pethig, R. R.; Goethe, J. W. V; Pethig, R. R. *Dielectrophoresis*; 2017. https://doi.org/10.1007/978-1-4614-5491-5 319.
- (77) Belkin, A.; Bezryadin, A.; Hendren, L.; Hubler, A. Recovery of Alumina Nanocapacitors after High Voltage Breakdown. *Sci. Rep.* **2017**, *7* (1), 1–8. https://doi.org/10.1038/s41598-017-01007-9.
- (78) Thoms, E.; Sippel, P.; Reuter, D.; Weiß, M.; Loidl, A.; Krohns, S. Dielectric Study on Mixtures of Ionic Liquids. *Sci. Rep.* **2017**, *7* (1), 1–9. https://doi.org/10.1038/s41598-017-07982-3.
- (79) Pethig, R. Review—Where Is Dielectrophoresis (DEP) Going? *J. Electrochem. Soc.* **2017**, *164* (5), B3049—B3055. https://doi.org/10.1149/2.0071705jes.
- (80) Çetin, B.; Li, D. Dielectrophoresis in Microfluidics Technology. *Electrophoresis*. 2011.

- https://doi.org/10.1002/elps.201100167.
- (81) Jones, T. B. Basic Theory of Dielectrophoresis and Electrorotation. *IEEE Eng. Med. Biol. Mag.* **2003**. https://doi.org/10.1109/MEMB.2003.1304999.
- (82) Velmanickam, L.; Laudenbach, D.; Nawarathna, D. Dielectrophoretic Label-Free Immunoassay for Rare-Analyte Quantification in Biological Samples. *Phys. Rev. E* 2016. https://doi.org/10.1103/PhysRevE.94.042408.
- (83) Hughes, M. P. Strategies for Dielectrophoretic Separation in Laboratory-on-a-Chip Systems. Electrophoresis. 2002. https://doi.org/10.1002/1522-2683(200208)23:16<2569::AID-ELPS2569>3.0.CO;2-M.
- (84) Dimaki, M.; Bøggild, P. Dielectrophoresis of Carbon Nanotubes Using Microelectrodes: A Numerical Study. *Nanotechnology* **2004**. https://doi.org/10.1088/0957-4484/15/8/039.
- (85) Chou, C. F.; Tegenfeldt, J. O.; Bakajin, O.; Chan, S. S.; Cox, E. C.; Darnton, N.; Duke, T.; Austin, R. H. Electrodeless Dielectrophoresis of Single- and Double-Stranded DNA. *Biophys. J.* **2002**. https://doi.org/10.1016/S0006-3495(02)73977-5.
- (86) Goater, A. D.; Pethig, R. Electrorotation and Dielectrophoresis. *Parasitology* **1998**. https://doi.org/10.1017/S0031182099004114.
- (87) Kadaksham, A. T. J.; Singh, P.; Aubry, N. Dielectrophoresis of Nanoparticles. *Electrophoresis* 2004. https://doi.org/10.1002/elps.200406092.
- (88) Zhang, C.; Khoshmanesh, K.; Mitchell, A.; Kalantar-Zadeh, K. Dielectrophoresis for Manipulation of Micro/Nano Particles in Microfluidic Systems. *Analytical and Bioanalytical Chemistry*. 2010. https://doi.org/10.1007/s00216-009-2922-6.
- (89) Gascoyne, P. R. C.; Vykoukal, J. Particle Separation by Dielectrophoresis. *Electrophoresis*. 2002. https://doi.org/10.1002/1522-2683(200207)23:13<1973::AID-ELPS1973>3.0.CO;2-1.
- (90) Lee, D.; Hwang, B.; Kim, B. The Potential of a Dielectrophoresis Activated Cell Sorter (DACS) as a next Generation Cell Sorter. *Micro Nano Syst. Lett.* **2016**. https://doi.org/10.1186/s40486-016-0028-4.
- (91) Gonga, G.; Li, B. Dielectric Properties of Bionanocomposites. In *Polymer Nanocomposites for Dielectrics*; 2017. https://doi.org/10.1201/9781315364490.
- (92) Lo, Y. J.; Lin, Y. Y.; Lei, U.; Wu, M. S.; Yang, P. C. Measurement of the Clausius-Mossotti Factor of Generalized Dielectrophoresis. *Appl. Phys. Lett.* **2014**. https://doi.org/10.1063/1.4866344.
- (93) Gierhart, B. C.; Howitt, D. G.; Chen, S. J.; Smith, R. L.; Collins, S. D. Frequency Dependence of Gold Nanoparticle Superassembly by Dielectrophoresis. *Langmuir* **2007**. https://doi.org/10.1021/la701472y.
- (94) Ehrlich, P. Dielectric Properties of Teflon from Room Temperature to 314-Degrees-C and from Frequencies of 10\_2 to 10\_5 c/S. *J. Res. Natl. Bur. Stand. (1934).* **1953**. https://doi.org/10.6028/jres.051.024.
- (95) Hwang, Y.; Sohn, H.; Phan, A.; Yaghi, O. M.; Candler, R. N. Dielectrophoresis-Assembled Zeolitic Imidazolate Framework Nanoparticle-Coupled Resonators for Highly Sensitive and Selective Gas Detection. *Nano Lett.* **2013**. https://doi.org/10.1021/nl4027692.
- (96) Salimi, E.; Braasch, K.; Butler, M.; Thomson, D. J.; Bridges, G. E. Dielectric Model for Chinese Hamster Ovary Cells Obtained by Dielectrophoresis Cytometry. *Biomicrofluidics* **2016**. https://doi.org/10.1063/1.4940432.
- (97) Mortadi, A.; El Melouky, A.; Chahid, E. G.; El Moznine, R.; Cherkaoui, O. Studies of the Clausius– Mossotti Factor. J. Phys. Stud. 2016.
- (98) Honegger, T.; Berton, K.; Picard, E.; Peyrade, D. Determination of Clausius-Mossotti Factors and Surface Capacitances for Colloidal Particles. *Appl. Phys. Lett.* **2011**. https://doi.org/10.1063/1.3583441.
- (99) Urdaneta, M.; Smela, E. Multiple Frequency Dielectrophoresis. *Electrophoresis* **2007**. https://doi.org/10.1002/elps.200600786.
- (100) Cui, L.; Holmes, D.; Morgan, H. The Dielectrophoretic Levitation and Separation of Latex Beads in Microchips. *Electrophoresis* **2001**. https://doi.org/10.1002/1522-2683(200110)22:18<3893::AID-ELPS3893>3.0.CO;2-2.
- (101) Gossett, D. R.; Weaver, W. M.; Mach, A. J.; Hur, S. C.; Tat, H.; Tse, K.; Lee, W.; Amini, H.; Carlo, D. Di. Label-Free Cell Separation and Sorting in Microfluidic Systems. **2010**, 3249–3267. https://doi.org/10.1007/s00216-010-3721-9.
- (102) Pethig, R.; Markx, G. H. Applications of Dielectrophoresis in Biotechnology. *Trends Biotechnol.* **1997**, *15* (10), 426–432. https://doi.org/10.1016/S0167-7799(97)01096-2.
- (103) Kim, U.; Qian, J.; Kenrick, S. A.; Daugherty, P. S.; Soh, H. T. Multitarget Dielectrophoresis Activated Cell Sorter. *Anal. Chem.* **2008**. https://doi.org/10.1021/ac8015938.
- (104) Pohl, H. A.; Crane, J. S. Dielectrophoresis of Cells. Biophys. J. 1971. https://doi.org/10.1016/S0006-

- 3495(71)86249-5.
- (105) Mulhall, H. J.; Labeed, F. H.; Kazmi, B.; Costea, D. E.; Hughes, M. P.; Lewis, M. P. Cancer, Pre-Cancer and Normal Oral Cells Distinguished by Dielectrophoresis. *Anal. Bioanal. Chem.* 2011. https://doi.org/10.1007/s00216-011-5337-0.
- (106) Patel, S.; Showers, D.; Vedantam, P.; Tzeng, T. R.; Qian, S.; Xuan, X. Microfluidic Separation of Live and Dead Yeast Cells Using Reservoir-Based Dielectrophoresis. *Biomicrofluidics* **2012**. https://doi.org/10.1063/1.4732800.
- (107) Markx, G. H.; Talary, M. S.; Pethig, R. Separation of Viable and Non-Viable Yeast Using Dielectrophoresis. *J. Biotechnol.* **1994**. https://doi.org/10.1016/0168-1656(94)90117-1.
- (108) Velmanickam, L.; Nawarathna, D. Design and Fabrication of a Dielectrophoretic Cell Trap Array. *Adv. Sci. Technol. Eng. Syst. J.* **2017**, *2* (1), 84–89. https://doi.org/10.1109/HICSS.2013.399.
- (109) Velmanickam, L.; Nawarathna, K. Dielectrophoretic Cell Isolation in Microfluidics Channels for High-Throughput Biomedical Applications. *IEEE Int. Conf. Electro Inf. Technol.* **2016**, *2016-Augus*, 302–306. https://doi.org/10.1109/EIT.2016.7535256.
- (110) Qian, C.; Huang, H.; Chen, L.; Li, X.; Ge, Z.; Chen, T.; Yang, Z.; Sun, L. Dielectrophoresis for Bioparticle Manipulation. *International Journal of Molecular Sciences*. 2014. https://doi.org/10.3390/ijms151018281.
- (111) Asbury, C. L.; Diercks, A. H.; Van Den Engh, G. Trapping of DNA by Dielectrophoresis. *Electrophoresis* **2002**. https://doi.org/10.1002/1522-2683(200208)23:16<2658::AID-ELPS2658>3.0.CO;2-O.
- (112) Velmanickam, L.; Bains, M.; Fondakowski, M. ILluminate-MiRNA: Paradigm for High-Throughput, Low-Cost, and Sensitive MiRNA Detection in Serum Samples at Point-of-Care. **2019**.
- (113) Swami, N.; Chou, C. F.; Ramamurthy, V.; Chaurey, V. Enhancing DNA Hybridization Kinetics through Constriction-Based Dielectrophoresis. *Lab Chip* **2009**. https://doi.org/10.1039/b910598k.
- (114) Gagnon, Z.; Senapati, S.; Chang, H. C. Optimized DNA Hybridization Detection on Nanocolloidal Particles by Dielectrophoresis. *Electrophoresis* **2010**. https://doi.org/10.1002/elps.200900473.
- (115) Demircan, Y.; Özgür, E.; Külah, H. Dielectrophoresis: Applications and Future Outlook in Point of Care. *Electrophoresis*. 2013. https://doi.org/10.1002/elps.201200446.
- (116) Ballantyne, G. R.; Holtham, P. N. Evaluation of the Potential for Using Dielectrophoresis to Separate Minerals. *Miner. Eng.* **2014**. https://doi.org/10.1016/j.mineng.2013.09.009.
- (117) Ballantyne, G. R.; Holtham, P. N. Application of Dielectrophoresis for the Separation of Minerals. *Miner. Eng.* **2010**. https://doi.org/http://dx.doi.org/10.1016/j.mineng.2009.09.001.
- (118) Olariu, M.; Arcire, A.; Plonska-Brzezinska, M. E. Controlled Trapping of Onion-Like Carbon (OLC) via Dielectrophoresis. *J. Electron. Mater.* **2017**. https://doi.org/10.1007/s11664-016-4870-1.
- (119) Ohtsuka, S.; Suetomi, H.; Hikita, M. Fundamental Properties of OFF-ON Resistance of a New Type Self-Recovering Fuse Operated by Dielectrophoresis. In *Conference Record of the International Power Modulator Symposium and High Voltage Workshop*; 2006. https://doi.org/10.1109/MODSYM.2006.365287.
- (120) Froude, V. E.; Zhu, Y. Dielectrophoresis of Functionalized Lipid Unilamellar Vesicles (Liposomes) with Contrasting Surface Constructs. *J. Phys. Chem. B* **2009**. https://doi.org/10.1021/jp808454w.
- (121) Allahrabbi, N.; Chia, Y. S. M.; Saifullah, M. S. M.; Lim, K. M.; Lanry Yung, L. Y. A Hybrid Dielectrophoretic System for Trapping of Microorganisms from Water. *Biomicrofluidics* **2015**. https://doi.org/10.1063/1.4922276.
- (122) Kim, W. B.; Park, S. J.; Min, B. K.; Lee, S. J. Surface Finishing Technique for Small Parts Using Dielectrophoretic Effects of Abrasive Particles. *J. Mater. Process. Technol.* 2004. https://doi.org/10.1016/j.jmatprotec.2004.01.010.
- (123) Luo, Q.; Zhang, X.; Wang, H.; Qian, Y. The Use of Non-Uniform Electrokinetics to Enhance in Situ Bioremediation of Phenol-Contaminated Soil. *J. Hazard. Mater.* 2005. https://doi.org/10.1016/j.jhazmat.2005.02.007.
- (124) Abbasi Monfared, M.; Sheikhi, M.; Kasiri, N.; Mohammadi, T. Experimental Investigation of Oil-in-Water Microfiltration Assisted by Dielectrophoresis: Operational Condition Optimization. *Chem. Eng. Res. Des.* **2018**. https://doi.org/10.1016/j.cherd.2018.08.002.
- (125) Thwar, P. K.; Linderman, J. J.; Burns, M. A. Electrodeless Direct Current Dielectrophoresis Using Reconfigurable Field-Shaping Oil Barriers. *Electrophoresis* **2007**. https://doi.org/10.1002/elps.200700373.
- (126) Chou, C. F.; Zenhausern, F. Electrodeless Dielectrophoresis for Micro Total Analysis Systems. *IEEE Eng. Med. Biol. Mag.* **2003**. https://doi.org/10.1109/MEMB.2003.1266048.
- (127) Regtmeier, J.; Eichhorn, R.; Viefhues, M.; Bogunovic, L.; Anselmetti, D. Electrodeless Dielectrophoresis for Bioanalysis: Theory, Devices and Applications. *Electrophoresis*. 2011. https://doi.org/10.1002/elps.201100055.

- (128) Sharma, H.; Wood, J. B.; Lin, S.; Corn, R. M.; Khine, M. Shrink-Induced Silica Multiscale Structures for Enhanced Fluorescence from DNA Microarrays. *Langmuir* **2014**. https://doi.org/10.1021/la501123b.
- (129) Ladik, L. S. G. B. J. The Effect of Electric Field on the Electronic Structure of DNA. I. Calculation of the Polarizability and of the Permanent Dipole Moment for the Nucleotide Bases and Base Pairs. *Quantum Chem.* **1969**, *3* (5), 621–634.
- (130) Morgan, H.; Hughes, M. P.; Green, N. G. Separation of Submicron Bioparticles by Dielectrophoresis. *Biophys. J.* **1999**. https://doi.org/10.1016/S0006-3495(99)76908-0.
- (131) Iqbal, A.; Arslan, S.; Okumus, B.; Wilson, T. J.; Giraud, G.; Norman, D. G.; Ha, T.; Lilley, D. M. J. Orientation Dependence in Fluorescent Energy Transfer between Cy3 and Cy5 Terminally Attached to Double-Stranded Nucleic Acids. *Proc. Natl. Acad. Sci.* 2008. https://doi.org/10.1073/pnas.0801707105.
- (132) Nawarathna, D.; Turan, T.; Wickramasinghe, H. K. Selective Probing of MRNA Expression Levels within a Living Cell. *Appl. Phys. Lett.* **2009**. https://doi.org/10.1063/1.3213343.
- (133) Jain, P. K.; El-Sayed, M. A. Plasmonic Coupling in Noble Metal Nanostructures. *Chem. Phys. Lett.* **2010**. https://doi.org/10.1016/j.cplett.2010.01.062.
- (134) Pethig, R. Dielectrophoresis: Using Inhomogeneous AC Electrical Fields to Separate and Manipulate Cells. *Crit. Rev. Biotechnol.* **1996**. https://doi.org/10.3109/07388559609147425.
- (135) Pethig, R.; Huang, Y.; Wang, X. B.; Burt, J. P. H. Positive and Negative Dielectrophoretic Collection of Coiloidal Particles Using Interdigitated Castellated Microelectrodes. *J. Phys. D. Appl. Phys.* **1992**. https://doi.org/10.1088/0022-3727/25/5/022.
- (136) Washizu, M.; Kurosawa, O. Electrostatic Manipulation of DNA in Microfabricated Structures. *IEEE Trans. Ind. Appl.* **1990**. https://doi.org/10.1109/28.62403.
- (138) L. Velmanickam, I. T. Lima and D. Nawarathna, "Achieving over million-fold fluorescence enhancement for biosensing applications," 2020 IEEE Research and Applications of Photonics in Defense Conference (RAPID), Miramar Beach, FL, USA, 2020, pp. 1-2, doi: 10.1109/RAPID49481.2020.9195707.
- (139) Joel Gersten, Abraham Nitzan; "Spectroscopic properties of molecules interacting with small dielectric particles". J. Chem. Phys. 1 August 1981; 75 (3): 1139–1152. https://doi.org/10.1063/1.442161
- (140) Daehan Yoo, Avijit Barik, Fernando de León-Pérez, Daniel A. Mohr, Matthew Pelton, Luis Martín-Moreno, and Sang-Hyun Oh, "Plasmonic Split-Trench Resonator for Trapping and Sensing", ACS Nano 2021 15 (4), 6669-6677, DOI: 10.1021/acsnano.0c10014
- (141) Cao, Z., Zhu, Y., Liu, Y., Dong, S., Chen, X., Bai, F., Song, S., Fu, J., Small, "Dielectrophoresis-Based Protein Enrichment for a Highly Sensitive Immunoassay Using Ag/SiO2 Nanorod Arrays" 2018, 14, 1703265. https://doi.org/10.1002/smll.201703265
- (142) Iris Elvira, Andrés Puerto, Gladys Mínguez-Vega, Adrián Rodríguez-Palomo, Alejandro Gómez-Tornero, Angel García-Cabañes, and Mercedes Carrascosa, "Micro-patterns of gold nanoparticles assembled by photovoltaic optoelectronic tweezers: application to plasmonic fluorescence enhancement," Opt. Express 30, 41541-41553 (2022)
- (143) Akinobu Yamaguchi, Takao Fukuoka, Ryo Takahashi, Ryohei Hara, Yuichi Utsumi, "Dielectrophoresisenabled surface enhanced Raman scattering on gold-decorated polystyrene microparticle in micro-optofluidic devices for high-sensitive detection", Sensors and Actuators B: Chemical, Volume 230, 2016, Pages 94-100, ISSN 0925-4005, https://doi.org/10.1016/j.snb.2016.02.023.
- (144) Giulia Barzan, Alessio Sacco, Luisa Mandrile, Andrea M. Giovannozzi, James Brown, Chiara Portesi, Morgan R. Alexander, Paul Williams, Kim R. Hardie, Andrea M. Rossi, "New frontiers against antibiotic resistance: A Raman-based approach for rapid detection of bacterial susceptibility and biocide-induced antibiotic cross-tolerance" Sensors and Actuators B: Chemical, Volume 309, 2020, 127774, ISSN 0925-4005, https://doi.org/10.1016/j.snb.2020.127774.
- (145) I-Fang Cheng, Chi-Chang Lin, Dong-Yi Lin, Hsien-Chang Chang; A dielectrophoretic chip with a roughened metal surface for on-chip surface-enhanced Raman scattering analysis of bacteria. Biomicrofluidics 1 September 2010; 4 (3): 034104. https://doi.org/10.1063/1.3474638
- (146) Avijit Barik, Lauren M. Otto, Daehan Yoo, Jincy Jose, Timothy W. Johnson, and Sang-Hyun Oh, "Dielectrophoresis-Enhanced Plasmonic Sensing with Gold Nanohole Arrays "Nano Letters 2014 14 (4), 2006-2012 DOI: 10.1021/nl500149h
- (147) Logeeshan Velmanickam, Dharmakeerthi Nawarathna, "Electric fields assisted fluorescence enhancement for microRNA biomarker detection in serum samples: strategies for combating cancer, obesity and addiction to opioid," Proc. SPIE 11020, Smart Biomedical and Physiological Sensor Technology XVI, 110200G (2 May 2019); https://doi.org/10.1117/12.2520312.

- (148) Avijit Barik, Sudhir Cherukulappurath, Nathan J. Wittenberg, Timothy W. Johnson, and Sang-Hyun Oh, "Dielectrophoresis-Assisted Raman Spectroscopy of Intravesicular Analytes on Metallic Pyramids" Analytical Chemistry 2016 88 (3), 1704-1710, DOI: 10.1021/acs.analchem.5b03719
- (149) Reza Salemmilani, Brian D. Piorek, Rustin Y. Mirsafavi, Augustus W. Fountain III, Martin Moskovits, and Carl D. Meinhart, "Dielectrophoretic Nanoparticle Aggregation for On-Demand Surface Enhanced Raman Spectroscopy Analysis" Analytical Chemistry 2018 90 (13), 7930-7936, DOI:10.1021/acs.analchem.8b00510
- (150) Christian Schäfer, Dieter P. Kern and Monika Fleischer, "Capturing molecules with plasmonic nanotips in microfluidic channels by dielectrophoresis", Lab on a Chip, 2015, 15, 1066, DOI: 10.1039/C4LC01018C.
- (151) Katrin H. P. Vu, Ming-Che Lee, Gerhard H. Blankenburg, Yu-Jen Chang, Ming-Lee Chu, Andreas Erbe, Leonardo Lesser-Rojas, Yun-Ru Chen, and Chia-Fu Chou, "Time-Evolved SERS Signatures of DEP-Trapped Aβ and Zn2+Aβ Peptides Revealed by a Sub-10 nm Electrode Nanoga", Analytical Chemistry 2021 93 (49), 16320-16329. DOI: 10.1021/acs.analchem.1c01521
- (152) Daniel David Galvan, Vidit Parekh, Erik Liu, E-Lin Liu, and Qiuming Yu, "Sensitive Bacterial Detection via Dielectrophoretic-Enhanced Mass Transport Using Surface-Plasmon-Resonance Biosensors", Analytical Chemistry 2018 90 (24), 14635-14642, DOI: 10.1021/acs.analchem.8b05137.
- (153) L. Velmanickam, I.T. Lima Jr., D. Nawarathna, "External low frequency electric fields maximize the fluorescence enhancement through light-metal-fluorophore interactions of target biomolecules," Proc. SPIE 10881, Imaging, Manipulation, and Analysis of Biomolecules, Cells, and Tissues XVII, 108810S (4 March 2019); https://doi.org/10.1117/12.2510137
- (154) J. S. Borchers, M. J. Clark, S. B. Van Scoy, R. K. Anand, ChemElectroChem 2024, 11, e202300345. https://doi.org/10.1002/celc.202300345
- (155) Y. Wu, H. Zhang, Y. Yue, S. Wang, Y. Meng, Controllable and Scaffold-Free Formation of 3D Multicellular Architectures Using a Bipolar Electrode Array. Adv. Mater. Technol. 2024, 2301626. https://doi.org/10.1002/admt.202301626
- (156) Wu, Yupan, Yue, Yuanbo, Zhang, Haohao, Ma, Xun, Zhang, Zhexin, Li, Kemu, Meng, Yingqi, Wang, Shaoxi, Wang, Xuewen, Huang, Wei, Three-dimensional rotation of deformable cells at a bipolar electrode array using a rotating electric field, 2024, 933-945, Lab on a Chip, vol-24, DOI 10.1039/D3LC00882G.
- (157) Huang, L., He, W. and Wang, W. (2019), A cell electro-rotation micro-device using polarized cells as electrodes. ELECTROPHORESIS, 40: 784-791. <a href="https://doi.org/10.1002/elps.201800360">https://doi.org/10.1002/elps.201800360</a>.
- (158) Zhao, Y., Brcka, J., Faguet, J. et al. Elucidating the mechanism governing cell rotation under DEP using the volumetric polarization and integration method. Biomed Microdevices 20, 81 (2018). https://doi.org/10.1007/s10544-018-0327-z.
- (159) Geka G, Kanioura A, Likodimos V, Gardelis S, Papanikolaou N, Kakabakos S, Petrou P. SERS Immunosensors for Cancer Markers Detection. Materials (Basel). 2023 May 15;16(10):3733. doi: 10.3390/ma16103733. PMID: 37241360; PMCID: PMC10221005.
- (160) Namhyun Choi, Hajun Dang, Anupam Das, Myeong Seong Sim, Il Yup Chung, Jaebum Choo, SERS biosensors for ultrasensitive detection of multiple biomarkers expressed in cancer cells, Biosensors ana Bioelectronics, Volume 164, 2020, 112326, https://doi.org/10.1016/j.bios.2020.112326.
- (161) Maryam Arabi, Abbas Ostovan, Zhiyang Zhang, Yunqing Wang, Rongchao Mei, Longwen Fu, Xiaoyan Wang, Jiping Ma, Lingxin Chen, Label-free SERS detection of Raman-Inactive protein biomarkers by Raman reporter indicator: Toward ultrasensitivity and universality, Biosensors and Bioelectronics, Volume 174, 2021, 112825, https://doi.org/10.1016/j.bios.2020.112825.
- (162) Abdelmonaim Azzouz, Lamia Hejji, Ki-Hyun Kim, Deepak Kukkar, Badredine Souhail, Neha Bhardwaj, Richard J.C. Brown, Wei Zhang, Advances in surface plasmon resonance—based biosensor technologies for cancer biomarker detection, Biosensors and Bioelectronics, Volume 197, 2022, <a href="https://doi.org/10.1016/j.bios.2021.113767">https://doi.org/10.1016/j.bios.2021.113767</a> (163) Aysa Rezabakhsh, Reza Rahbarghazi, Farzaneh Fathi, Surface plasmon resonance biosensors for detection of Alzheimer's biomarkers; an effective step in early and accurate diagnosis, Biosensors and Bioelectronics, Volume 167, 2020, <a href="https://doi.org/10.1016/j.bios.2020.112511">https://doi.org/10.1016/j.bios.2020.112511</a>.
- (164) Jazayeri, M.H., Aghaie, T., Nedaeinia, R. et al. Rapid noninvasive detection of bladder cancer using survivin antibody-conjugated gold nanoparticles (GNPs) based on localized surface plasmon resonance (LSPR). Cancer Immunol Immunother 69, 1833–1840 (2020). <a href="https://doi.org/10.1007/s00262-020-02559-y">https://doi.org/10.1007/s00262-020-02559-y</a>